nature reviews earth & environment

https://doi.org/10.1038/s43017-025-00715-5

Review article

Check for updates

Ocean stratification in a warming climate

Lijing Cheng[1], Guancheng Li[2], Shang-Min Long[3,4], Yuanlong Li[5], Karina von Schuckmann[6], Kevin E. Trenberth[7,8], Michael E. Mann[9], John Abraham[10], Yan Du[11], Xuhua Cheng[3,4], Hailong Liu[12], Zhenhua Xu[5,13], Maofeng Liu[14], Qihua Peng[15], Xun Gong[16,17], Zhanhong Ma[18] & Huifeng Yuan[19]

Abstract

The ocean is highly stratified. Warm, fresh water sits on top of cold, salty water, influencing vertical oceanic exchange of heat, carbon, oxygen and nutrients. In this Review, we examine observed and projected stratification shifts and their impacts. Changes in ocean temperature and salinity have altered the ocean density field, leading to a 0.8 ± 0.1% dec^{-1} (90% confidence interval) increase in stratification in the global upper 2,000 m since the 1960s. These increases are most pronounced in the tropics and are primarily temperature driven. Model simulations project ongoing stratification increases in the future, with global 0–2,000 m stratification increasing 0.7 [0.3,1.1; 13–87% confidence interval], 1.4 [0.9,1.8] and 2.9 [2.1,3.8]% dec^{-1} by 2090–2100 relative to 2010–2020 under Shared Socioeconomic Pathways SSP1-2.6, SSP2-4.5 and SSP5-8.5, respectively; regional patterns of projected stratification changes generally follow observed trends. These observed and projected ocean stratification changes have important climate and ecological consequences, including alterations in ocean heat uptake, ocean currents, vertical mixing, tropical cyclone intensity, marine ecosystems and elevation of marine extremes. Further research should better quantify stratification change at critical layers and understand their drivers and impacts.

Sections

A full list of affiliations appears at the end of the paper. e-mail: chenglij@mail.iap.ac.cn

Introduction

Ocean stratification describes the layering of seawater, as dictated by temperature, salinity and thereby density (Fig. 1). Warmer, fresher (less dense) water sits atop cooler, saltier (denser) water. As stratification strength changes with depth, several distinct layers form[1] (Fig. 1): a mixed layer, with vertically homogeneous density (very weak stratification) that directly experiences the effects of air–sea exchanges; a 'barrier layer', separating a shallow salinity-dominated mixed layer from a deeper isotherm layer; and thermocline, halocline and pycnocline that separate the upper mixed layer and deeper ocean, marked by pronounced vertical gradients in temperature, salinity and density, respectively (Fig. 1). This stratification establishes stable conditions, limiting convection and acting as a barrier to vertical mixing[2], in turn regulating exchange of heat, momentum, carbon, oxygen and nutrients.

There are many ways that stratification can be defined. The most common is the Brunt–Väisälä frequency (N^2), representing the intrinsic frequency of a displaced water parcel. It is calculated as:

$$N^2 = g\left[-\left(\frac{1}{\rho}\right)\left(\frac{\partial \sigma_n}{\partial z}\right)\right] \quad (1)$$

where ρ, σ_n and g denote seawater density, local potential density anomaly and gravity acceleration, respectively. The more stratified the water column, the higher the static stability and the higher the buoyancy frequency. N^2 can be calculated over different layers. Other definitions or indices have also been used, either for simplicity or to highlight different dynamical conditions. These include: temperature or density difference between the surface and 200 m depth[3,4]; N^2 averaged from 0 to 2,000 m (ref. 5); density difference at the bottom of the mixed layer[6] (pycnocline); or potential energy anomaly[7–9], defined by vertical integral of density anomalies (relative to a vertical mean density) over a certain depth. There is no complete consistency among these definitions[10].

Given stratification sensitivity to temperature and salinity, anthropogenically forced climate changes have driven regional and global shifts in stratification. Indeed, stronger surface-level warming relative to deeper layers[11–13], coupled with changes in salinity associated with an amplified global hydrological cycle[14–16], has resulted in a robust increase in stratification; ocean dynamics (circulation, eddies and mixing) and Earth system interactions have also contributed. Since 1970, this increase has been ~0.8–1.0% dec^{-1} at 0–200 m depth[17,18], a change that is also expected into the future[4]. However, as the upper ocean responds faster than the deeper ocean to greenhouse gas forcing, and in ways that are nearly irreversible[19,20], asynchronous changes in the surface and subsurface oceans are expected.

This increase in ocean stratification has numerous climate implications. Higher stratification results in decreased ocean mixing[2] and ocean ventilation, in turn reducing vertical exchange of ocean heat[21,22], carbon[23,24], nutrients[25] and oxygen[26]. The reduced ocean vertical heat and carbon exchange leads to more heat piled up in the near-sea-surface layer and more CO_2 in the air, thereby exacerbating the speed and magnitude of Earth's surface warming. These processes provide critical feedback to climate change[22]. The increased stratification also reduces vertical oxygen exchange and exacerbates deoxygenation, putting ocean life at risk[27,28]. In particular, the oxygen minimum zones are expanding in the tropical and North Pacific, North Indian and equatorial Atlantic oceans[29], compressing the habitats of macro-organisms, with negative impacts for fisheries[30], and also enhancing the production of nitrous oxide, a strong greenhouse gas[31]. Thus, understanding how and why ocean stratification changes is vital for constraining climate change and supporting climate action.

In this Review, we outline how ocean stratification has varied, and will vary, with a warming climate. We begin by outlining the basic structure of ocean density, stratification, and its seasonal and regional variations. We next outline contemporary global and regional changes from observational products, before discussing future projected changes from climate models. The far-reaching consequences of ocean stratification change on Earth's physical and biological systems are subsequently discussed. We close with a discussion of the remaining challenges and research needs. Throughout, stratification is defined by the Brunt–Väisälä frequency (except pycnocline stratification, which is defined as density gradient 15 m below the bottom of mixed layer, as in ref. 6).

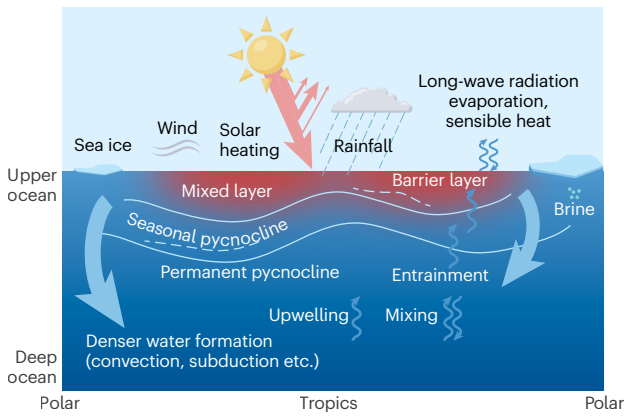

Fig. 1 | Explaining ocean stratification. A schematic representation of the processes and features of ocean stratification. Ocean stratification arises from many dynamic and thermodynamic processes, creating stable ocean conditions that limit vertical mixing.

The regional and seasonal variation of ocean stratification

Ocean stratification forms a distinct vertical feature depending on the structure of temperature, salinity and density. Global-mean ocean density increases from ~24.3 kg m^{-3} (density values are subtracted by 1,000 throughout this paper) near the surface to ~27.1 kg m^{-3} at 500 m, with the strong gradient occurring within ~20–200 m (the pycnocline). The numbers correspond to a positive N^2, with a peak of ~2.2×10^{-4} s^{-2} (Fig. 2a–c). Thus, stratification of the upper ocean (0–200 m; Fig. 2a) is generally stronger than that of the deep ocean (200–500 m; Fig. 2b). Such vertical stratification is dominated by temperature structure decreasing from ~19 °C at the sea surface to ~8 °C at 500 m (Fig. 2c). Above ~150 m, the salinity structure reinforces this thermal effect because of the fresher water near the surface, but from ~150 to 500 m, salinity structure compensates the thermal stratification (Fig. 2c).

Ocean stratification is also characterized by prominent regional differences (Fig. 2): N^2 for the upper 200 m is stronger in the tropical regions than middle and high latitudes, whereas N^2 for 200–500 m is strongest in the subtropics, both associated with the location of pycnocline (Fig. 2a,b). The tropics generally feature strong stratification in the upper ~200 m (Fig. 2a,b). In all tropical regions, a sharp thermocline and pycnocline are present owing to surface solar heating and upwelling of cooler subsurface waters. The absent seasonality in solar heating

(the Sun always moves between the tropics of Cancer and Capricorn) translates to minimal stratification seasonality[3].

Within the tropics, differences in stratification characteristics emerge from contrasting drivers and mechanisms. In the tropical Pacific, for example, the thermocline and pycnocline are typically deeper in the west (100–200 m; Fig. 2d) than in the east (<100 m; Fig. 2e), causing shallower but stronger N^2 maximum (~7×10^{-4} s^{-2} at <100 m) in the East Pacific (Fig. 2d,e). This difference is shaped by the trade winds which drive strong cold-water upwelling in the East Pacific confronting the near-surface warm water — a process critical in regulating characteristics of the El Niño–Southern Oscillation (ENSO)[32,33]. Specifically, the strength and depth of the thermocline and pycnocline are key factors determining the ocean–atmosphere coupling strength, for instance through the thermocline feedbacks[34].

Elsewhere in the tropics, the Intertropical Convergence Zone (ITCZ) and monsoon regions are characterized by near-surface salinity stratification. In such regions of heavy rainfall and terrestrial runoff, a salt-stratified boundary layer — typically several to tens of metres in thickness and uniform in temperature — forms beneath the mixed layer[35,36]. Thus, upper ocean N^2 structure in the western tropical Pacific (Fig. 2d), the Bay of Bengal[37] (Fig. 2f) and the Amazon plume[38] (Fig. 2g) correspond more strongly to salinity than to temperature. Maximum N^2 can reach ~8×10^{-4} s^{-2} in the Amazon plume near the surface in boreal summer because of the river discharge. By inhibiting vertical exchange between the warm mixed layer and the cold waters below the thermocline waters, the barrier layer maintains the warm tropical sea surface temperature (SST) and amplifies its variability[39–41].

Unlike in other tropical regions, however, semiannual variations in stratification characteristics are evident in the ITCZ and monsoon regions. For example, the mixed layer in the Bay of Bengal (Fig. 2f) is relatively deep during the summer and winter monsoons but shallow in inter-monsoon seasons[41,42], as regulated by wind-driven near-surface turbulent mixing. In addition, monsoons also affect ocean salinity stratification through surface freshwater fluxes (rainfall and river discharge) and freshwater transport by monsoonal ocean circulations[43,44].

In the mid-latitude oceans, stratification is regulated by the seasonal mitigation of surface solar radiation. Thus, near-surface stratification strengthens in summer and weakens in winter, as seen in the Gulf Stream (Fig. 2h) and Northwest Pacific (Fig. 2i). This feature is discernible in the evolution of the mixed-layer depth, which is typically large in late winter[45], and the subsequent shoaling of mixed-layer depth detrains the mixed-layer water with surface properties into the subsurface ocean[46] — a process known as subduction that governs the formation of water masses[47]. Associated with the seasonal changes of the mixed layer, the seasonal pycnocline forms beneath the mixed layer in summer in the mid and high latitudes and is likely to merge intermittently with the permanent pycnocline in winter (Fig. 2h). The thermocline and pycnocline have essential roles in configuring the wind-driven circulation of the upper ocean[48,49]. They affect the heat and material (for instance, freshwater, carbon and oxygen) budgets of the mixed layer via entrainment — a process involving mixed-layer deepening and merging cold and nutrient-rich thermocline waters into the mixed layer.

In the high latitudes, ocean salinity is vital for ocean stratification. Antarctic (Fig. 2j) and Arctic (Fig. 2k) waters are predominantly stratified by salinity and feature a halocline rather than a thermocline: relatively cold, fresh water tops warmer, salty subsurface water[50]. Brine is rejected as sea ice forms, leaving saltier, denser waters behind; waters are correspondingly freshened as sea ice and icebergs melt[51]. The salinity-governed high-latitude stratification tends to suppress upward heat transport to the surface and thereby modulates local interactions between air and sea ice. The melting and freezing of sea ice, therefore, regulate the high-latitude water cycle and mediate effects of the wind stress acting at the surface[50], shaping the seasonality of regional stratification. In marginal seas of the subpolar Atlantic and around Antarctica, weak winter stratification coupled with mixed-layer depths reaching thousands of metres facilitates deep convection. These characteristics in stratification enable the formation of North Atlantic Deep Water and Antarctic Bottom Water — primary drivers of the Atlantic Meridional Overturning Circulation (AMOC)[52] and the global conveyor belt[53].

Observed stratification changes

Marked stratification changes have been observed since 1960 (Fig. 3). Several gridded datasets are available to quantify these changes, including those of Cheng[54,55], Ishii[56], Levitus[57], Sallée[6] and Yamaguchi[3]. Given their improved subsurface data and processing methodologies[12], subsequent discussion focuses on the average of the Cheng, Ishii and Levitus datasets to examine global and regional ocean stratification changes. Unless otherwise stated, uncertainty represents 90% confidence intervals, summer represents August–October in the Northern Hemisphere and January–March in the Southern Hemisphere[6], and winter represents August–October in the Southern Hemisphere and January–March in the Northern Hemisphere.

Observed global stratification changes

As a global average, stratification has robustly increased across all levels (Table 1 and Fig. 3). This enhanced stratification arises from stronger warming near the sea surface compared with the deep ocean[5,12]. The magnitude of the changes, however, varies depending on the stratification layer considered, as well as the season.

Notable changes are apparent for stratification defined over 0–200 m depth (Fig. 3a). From 1960 to 2024, stratification increased by $6.9 \pm 1.5 \times 10^{-6}$ s^{-2} (or $1.1 \pm 0.2\%$ dec^{-1}, where the percentage change is relative to a 2005–2020 climatology) as an average of the three datasets[54,56,57] (Table 1); individual dataset trends are consistent (Supplementary Table 2). This trend is larger than the 0.78–0.86% dec^{-1} previously reported[17] (Supplementary Table 3), largely owing to differences in data selection (EN4 data used in ref. 17 underestimate long-term ocean warming[58,59]) and the time period examined (1970–2017). Additional estimates with different approaches based on individual profiles rather than gridded datasets are broadly similar at 0.6–1.1% dec^{-1} (ref. 3) and $1.3 \pm 0.3\%$ dec^{-1} (ref. 6) (Supplementary Table 3), the differences again largely reflecting contrasting methodologies. Seasonally, the absolute changes from 1960 to 2024 are more pronounced in summer than winter ($8.8 \pm 1.7 \times 10^{-6}$ s^{-2} versus $4.9 \pm 1.5 \times 10^{-6}$ s^{-2}) but the percentage increases relative to 2005–2020 are broadly consistent ($1.2 \pm 0.2\%$ dec^{-1} versus $1.0 \pm 0.3\%$ dec^{-1}) because of stronger climatological stratification in summer (Table 1, Supplementary Table 2 and Supplementary Fig. 1).

Stratification over 0–2,000 m, representing the contrast of surface and deep water, has also increased. Since 1960, annual mean stratification increased $0.9 \pm 0.1 \times 10^{-6}$ s^{-2} or $0.8 \pm 0.1\%$ dec^{-1} (Table 1 and Fig. 3b), with estimates again consistent across datasets[5] (Supplementary Table 2). In absolute terms, seasonal changes are much smaller relative to 0–200 m (Table 1), but the percentage increases are fairly consistent at $0.9 \pm 0.1\%$ dec^{-1} for summer and $0.8 \pm 0.2\%$ dec^{-1} for winter (Supplementary Table 2 and Supplementary Fig. 2). No other estimates of changes at 0–2,000 m have been evaluated (Supplementary Table 3).

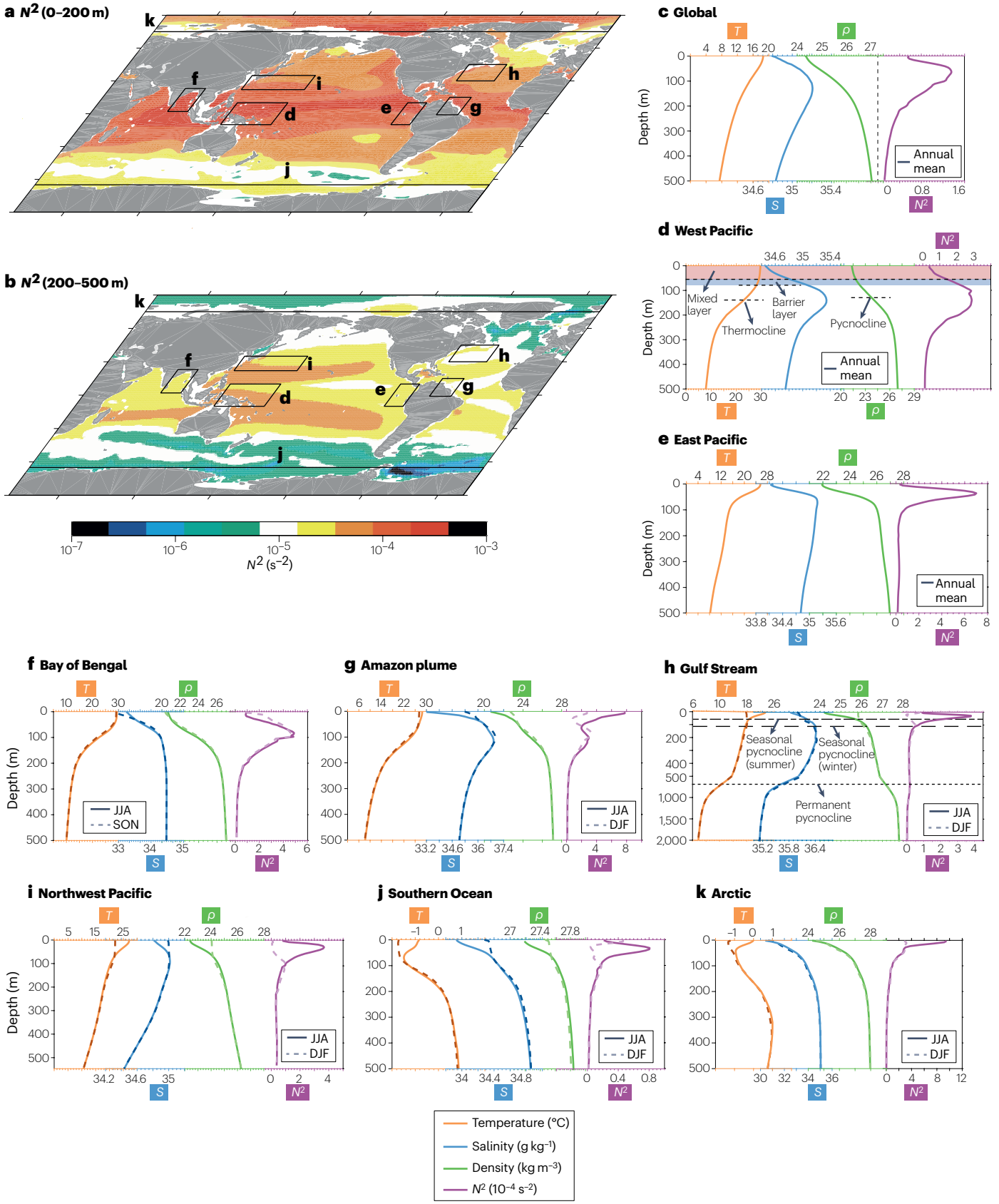
a N^2 (0–200 m)
b N^2 (200–500 m)
k
f
i
h
d
e
g
j
10^{-7}
10^{-6}
10^{-5}
10^{-4}
10^{-3}
N^2 (s^{-2})
c Global
d West Pacific
e East Pacific
Depth (m)
T
ρ
S
N^2
Annual mean
Mixed layer
Barrier layer
Thermocline
Pycnocline
f Bay of Bengal
g Amazon plume
h Gulf Stream
JJA
SON
DJF
Seasonal pycnocline (summer)
Seasonal pycnocline (winter)
Permanent pycnocline
i Northwest Pacific
j Southern Ocean
k Arctic
Temperature (°C)
Salinity (g kg^{-1})
Density (kg m^{-3})
N^2 (10^{-4} s^{-2})

Fig. 2 | Global and regional ocean stratification. **a**, Stratification (the square of the buoyancy frequency; N^2) at 0–200 m depth. **b**, As in panel **a**, but for 200–500 m depth. **c**–**e**, Annual-mean temperature (T), salinity (S), density (ρ) and stratification (N^2) profiles averaged over the globe (panel **c**), the West Pacific (panel **d**; boxed area labelled '**d**') and the East Pacific (panel **e**; boxed area labelled '**e**'). **f**–**k**, Seasonal-mean T, S, ρ and N^2 profiles averaged over the Bay of Bengal (panel **f**; boxed area labelled '**f**'), the Amazon Plume (panel **g**; boxed area labelled '**g**'), the Gulf Stream (panel **h**; boxed area labelled '**h**'), the Northwest Pacific (panel **i**; boxed area labelled '**i**'), the Southern Ocean (panel **j**; boxed area labelled '**j**') and the Arctic Ocean (panel **k**; boxed area labelled '**k**'). Seasonal means are calculated over June–August (JJA; solid lines) and December–February (DJF; dashed lines), except for the Bay of Bengal where DJF is replaced with September–November (SON). All panels represent the average of two observational products[54,56] over 2005–2020. Stratification tends to decrease with depth, but there is marked regional variability.

Comparatively larger-magnitude stratification changes are apparent in the seasonal pycnocline. Defined as N^2 computed from density gradient over the 15-m layer directly below the mixed-layer base[6], stratification in the pycnocline increased by $16.8 \pm 3.2 \times 10^{-6}\,s^{-2}$ or $1.8 \pm 0.3\%\ dec^{-1}$ for the ensemble average of the three gridded datasets (Table 1, Fig. 3c and Supplementary Table 2). However, an individual estimate based on in situ profiles and a linear regression method suggests a substantially larger increase of $8.9 \pm 2.7\%\ dec^{-1}$ (ref. 6). This diversity highlights substantial uncertainty in estimating pycnocline stratification, largely related to inadequate spatiotemporal data sampling[54] and estimates of pycnocline depth[60]. Stronger seasonal pycnocline stratification occurs in summer ($1.7 \pm 0.4\%\ dec^{-1}$) compared with winter ($1.0 \pm 0.7\%\ dec^{-1}$) (Table 1, Supplementary Table 2 and Supplementary Fig. 3), with large wintertime uncertainty linked to the difficulty in determining the pycnocline. In all layers, these seasonal differences in stratification trends are linked to human-induced amplification of the SST annual cycle outside of the tropics: in summer, decreasing mixed-layer depth leads to more efficient heat trapping in the upper ocean, yielding a larger SST and stratification increase than in winter[61–63]. Changes in the seasonal cycle of precipitation (linked to both water vapour and atmospheric circulation changes[64]) could also be important, although observational evidence is incomplete[65].

Observations also reveal remarkable interannual and decadal variations in global upper-ocean stratification (Fig. 3). This interannual variability is dominant in the tropics and shows positive correlations with ENSO (Fig. 3a, inset); ENSO strongly alters global ocean temperature, salinity, mixed layer, boundary layer and thermocline[66–68]. However, stratification variability in the North Indian Ocean is negatively linked to the Indian Ocean Dipole[69,70]. Globally, decadal variations are correlated with Atlantic Multidecadal Variability and Pacific Decadal Variability (PDV), largely through changes in sea surface properties[3,5,71] (Supplementary Fig. 4), but the North Atlantic Oscillation is important in driving decadal stratification variability in the North Atlantic Ocean[3].

Observed regional stratification changes

Strengthened stratification is not just a feature of global mean, but a pervasive signal observed across much of the oceans (Fig. 4). Indeed, ~82.6% and ~92.0% of global ocean grids (at 1° × 1°) show enhanced stratification since 1960 for the 0–200 m and 0–2,000 m layers, respectively[3–5] (Fig. 4a,f); in the pycnocline, this value is lower at ~75.7%, associated with its dynamical complexity (Fig. 4k). In most cases, temperature changes dominate the observed stratification signals (Fig. 4b,g,l), contributing 85.2%, 97.2% and 65.3% of the increases at 0–200 m, 0–2,000 m and the pycnocline, respectively. Salinity changes have a secondary role (Supplementary Fig. 5), but can be important locally (Fig. 4c,h,m).

More regionally, strong differences in stratification are apparent across all levels, particularly between lower and higher latitudes. Generally, stratification increases are larger in the tropics compared with the middle and high latitudes (except the Arctic) in all three major basins[3,6,8] (Fig. 4a,f,k and Supplementary Fig. 6). Tropical stratification increases are mainly associated with contrasting temperature trends between surface and deep layers (Fig. 4a,f,k and Supplementary Fig. 6). Specifically, this enhanced stratification represents the effects of near-surface warming (driven by strong anthropogenic heat gain and intensified subtropical gyres[72]) and near-thermocline cooling[5] (driven by enhanced Ekman pumping[73] and anomalous advection[74]); wind stress and buoyancy forcing are both important for shoaling the equatorial thermocline[75,76].

Of course, more localized differences are also evident, highlighting the varied contributions of temperature and salinity. For instance, pronounced and significant stratification increases in the West Pacific Warm Pool at 0–200 m and 0–2,000 m (Fig. 4a,f) are largely temperature-driven (Fig. 4b,c,g,h) through intensified trade winds[77,78]. In contrast, tropical eastern Pacific and Atlantic stratification increases (also statistically significant) mainly occur in the pycnocline layer (Fig. 4k), where the temperature and salinity contributions are comparable (Fig. 4l,m). Here, salinity reinforces the temperature effects because of increased precipitation minus evaporation, and surface ocean freshening[14,15].

Compared with the tropics, stratification changes in the extratropics tend to be smaller (Fig. 4a,f,k and Supplementary Fig. 6). In the Atlantic, upper 200 m stratification since 1960 varies from $7.7 \pm 5.5 \times 10^{-6}\ s^{-2}$ ($0.7 \pm 0.5\%\ dec^{-1}$) in the tropics (10° S–10° N) to $3.8 \pm 1.8 \times 10^{-6}\ s^{-2}$ ($0.8 \pm 0.4\%\ dec^{-1}$) in the mid-latitudes (10–50° N/S). For 0–2,000 m stratification, the increase in the tropics is $1.1 \pm 0.6 \times 10^{-6}\ s^{-2}$ ($0.7 \pm 0.4\%\ dec^{-1}$) since 1960, also larger than in the mid-latitudes with $0.7 \pm 0.1 \times 10^{-6}\ s^{-2}$ ($0.8 \pm 0.1\%\ dec^{-1}$). These changes — which are typically weaker than those in other basins — highlight the offsetting effects of temperature and salinity. For instance, within 50° S to 50° N of the Atlantic Ocean, salinity changes offset ~31.1% of the temperature-induced stratification increase for the 0–2,000-m average[5] (Fig. 4f–h). Salinity changes in these regions are primarily caused by increased evaporation-minus-precipitation associated with an amplified water cycle[16], although salt redistribution by changes in ocean circulation (such as the AMOC) and water masses are also important[79,80]. In the Pacific Ocean, tropical stratification at 0–200 m and 0–2,000 m since 1960 are $11.1 \pm 4.7 \times 10^{-6}\ s^{-2}$ ($1.2 \pm 0.5\%\ dec^{-1}$) and $1.3 \pm 0.4 \times 10^{-6}\ s^{-2}$ ($0.8 \pm 0.2\%\ dec^{-1}$), respectively, slightly larger than the extratropics (for 0–200 m $4.8 \pm 1.0 \times 10^{-6}\ s^{-2}$ or $1.5 \pm 0.3\%\ dec^{-1}$; for 0–2,000 m $0.9 \pm 0.2 \times 10^{-6}\ s^{-2}$ or $1.2 \pm 0.2\%\ dec^{-1}$). The difference is primarily because of the strong temperature contribution and secondary salinity contribution in the tropical West, Northeast and Northwest Pacific (Fig. 4b,g,l), different from the Atlantic where salinity dominates (Fig. 4c,h,m). However, for all basins, the percentage change is always larger in the extratropics than the tropics because of the much stronger mean stratification in the tropics (Fig. 2).

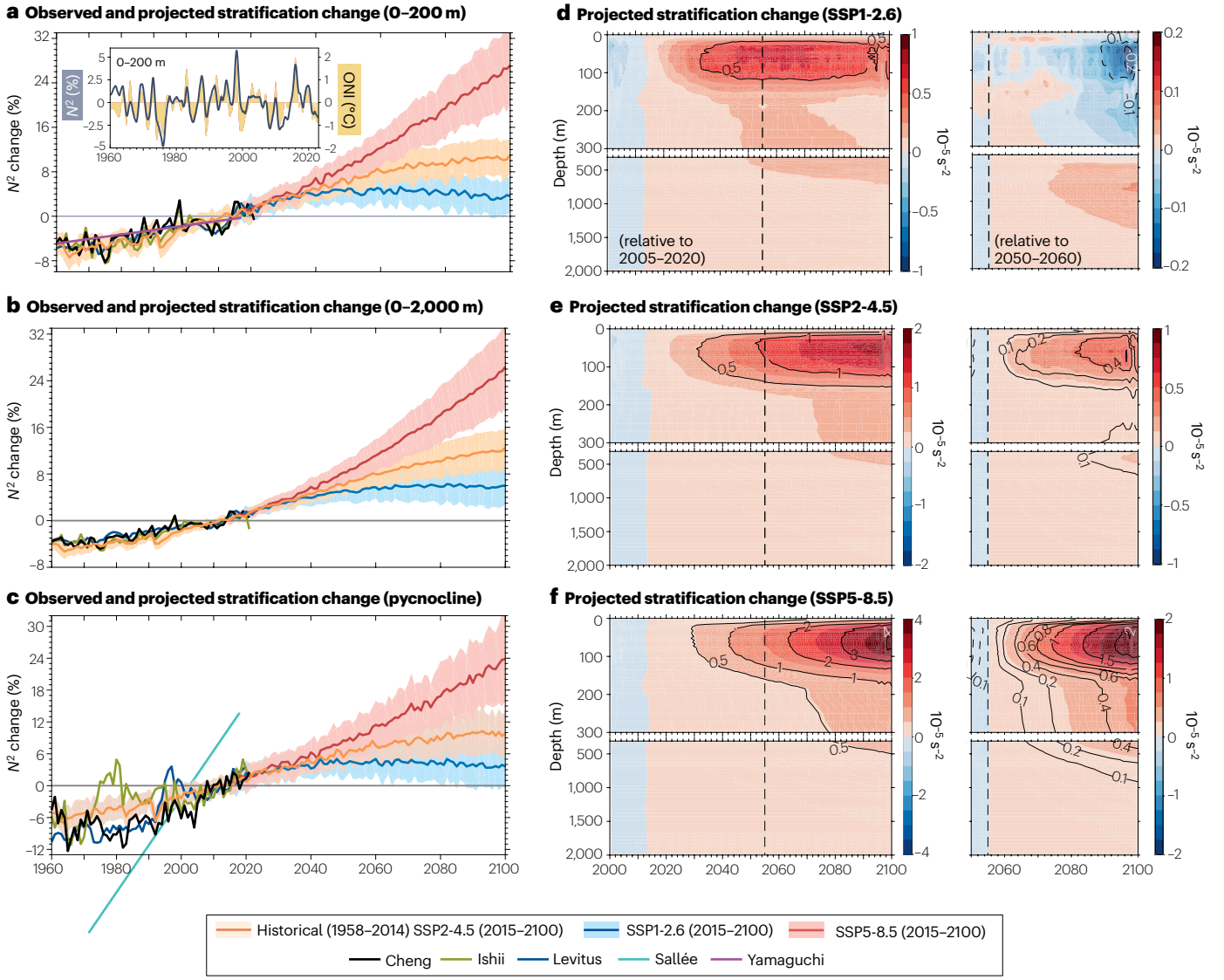

Fig. 3 | Observed and projected global ocean stratification changes. **a**, Stratification time series at 0–200 m depth from various observational products[54,56,57] and CMIP6 simulations[90] under different Shared Socioeconomic Pathways (SSPs), all relative to a 2005–2020 baseline. For projections, the bold line represents the ensemble mean and shading the model spread (±1σ). The inset displays the observed detrended stratification time series alongside the oceanic Niño3.4 index (ONI)[248]. **b**, As in panel **a**, but for stratification at 0–2,000 m depth. **c**, As in panel **a**, but for stratification change at the pycnocline. **d**, Global-mean and ensemble-mean stratification changes relative to 2005–2020 (left) and 2050–2060 (right) for SSP1-2.6. **e**, As in panel **d** but for SSP2-4.5. **f**, As in panel **d** but for SSP5-8.5. Note the different colour bar scales in panels **d**–**f**. Observations indicate a robust increase in ocean stratification, but its continued evolution depends on the emissions pathway.

There are also strong contrasts in stratification signals between the northern and southern high latitudes. Overall, pronounced stratification increases are evident in the Arctic Ocean (north of 70° N) in all levels (Fig. 4a,f,k): $7.6 \pm 7.5 \times 10^{-6}$ s^{-2} ($0.7 \pm 0.7\%$ dec^{-1}) and $1.3 \pm 1.2 \times 10^{-6}$ s^{-2} ($0.7 \pm 0.7\%$ dec^{-1}) for 0–200 m and 0–2,000 m, respectively. Here, the increases are dominated by salinity changes (Fig. 4c,h,m and Supplementary Fig. 6), specifically freshening associated with sea-ice and land-ice melt[81–84]. In the Southern Ocean (south of 50° S), by contrast, changes are far more subdued, with pockets of statistically significant decreases in stratification since 1960 (Fig. 4a,f,k). These stratification decreases largely reflect temperature effects (Fig. 4b,g,l), notably surface cooling and subsurface warming[12,85,86], that reduce stratification. The absence of near-surface warming is attributed to continuous northward heat transport and wind-driven upwelling of unmodified water from depth[85,87]. Subsurface warming is associated with the subduction and advection of warm waters[87] and the reduced formation rate of the bottom water[82,88]. Moreover, wind-driven northward transport of sea ice and freshwater increases salinity stratification, reduces vertical mixing, and contributes to surface and subsurface temperature trends, especially around West Antarctica[81].

In general, stratification changes are consistently stronger and more statistically significant in local summer (Fig. 4d,i,n) compared with winter (Fig. 4e,j,o and Supplementary Fig. 6). These characteristics are particularly observable outside the tropics given limited seasonal changes in climatological mixed-layer depths within the tropics. The most notable seasonal change occurs in the North Pacific, where much stronger summer pycnocline stratification ($84.1 \pm 24.4 \times 10^{-6}\,s^{-2}$ or $2.9 \pm 0.8\%\ dec^{-1}$ within 30–60° N) occurs relative to winter ($9.3 \pm 4.0 \times 10^{-6}\,s^{-2}$ or $3.5 \pm 1.5\%\ dec^{-1}$). The Gulf Stream and its extension regions also show strong seasonal differences. These changes are mainly caused by the amplification of the SST seasonal cycle in the mid-latitudes associated with large summertime SST increases and stronger decreases of the summer mixed-layer depth relative to winter[61,89].

Projected stratification changes

With observations indicating robust increases in stratification across the global oceans, it is prudent to assess how stratification might evolve further into the future. Doing so requires the use of model simulations, with Coupled Model Intercomparison Project Phase 6 (CMIP6)[90] models being the most comprehensive and complete. Although suffering from biases (Supplementary Figs. 1–3, 6–9), CMIP6 models tend to perform well in simulating ocean stratification change in the upper 2,000 m since 1960 and some key spatial features. Focusing on robust features in the multimodel mean, stratification changes at 0–200 m, 0–2,000 m and the pycnocline are now assessed up to 2100 under different Shared Socioeconomic Pathways, including SSP1-2.6 (a low-emission scenario), SSP2-4.5 (a moderate-emission scenario) and SSP5-8.5 (a high-emission scenario)[18,91].

Projected global stratification changes

The CMIP6 multimodel mean suggests that the observed increase in ocean stratification will continue into the twenty-first century (Fig. 3). These increases are consistent with previous-generation climate models[4,24,92]. Across all definitions, the stratification increases up to 2050–2060 regardless of the emission scenario (Fig. 3a–c). For instance, relative to 2010–2020, 0–200 m stratification changes are 1.0 [0.6,1.4], 1.7 [1.2,2.1] and 2.5 [2.0,3.1]% dec^{-1} for SSP1-2.6, SSP2-4.5 and SSP5-8.5, respectively (Table 1). Changes for 0–2,000 m stratification (1.2 [0.8,1.6], 1.7 [1.2,2.1] and 2.3 [1.7,2.8]% dec^{-1}) and the pycnocline stratification (1.0 [0.5,1.5], 1.6 [1.1,2.1] and 2.2 [1.5,3.1]% dec^{-1}) are also similar (Table 1 and Fig. 3).

After 2050, however, divergent trajectories of future stratification emerge. For instance, under SSP1-2.6, changes by 2090–2100 (relative to 2050–2060) are −0.3 [−0.5,0.0]% dec^{-1} at 0–200 m and 0.1 [−0.2,0.5]% dec^{-1} at 0–2,000 m, revealing a stabilization of stratification changes after the 2050s (Fig. 3b). This change relates to the different response times of upper and deep ocean: fast upper and slow deep ocean responses[93,94]. Whereas mixed-layer temperature stabilizes in the middle of this century (Fig. 3d and Supplementary Fig. 9), the deep ocean continues absorbing heat because of a remaining energy imbalance, producing a warming contrast between the upper and deep ocean[19].

Yet, under moderate and high-emission scenarios, stratification at 0–2,000 m continues. Indeed, within 2090–2100 (relative to 2050–2060), stratification increases at this level reach 1.2 [0.7,1.6]% dec^{-1} and 3.6 [2.5,4.8]% dec^{-1} for SSP2-4.5 and SSP5-8.5, respectively (Table 1). Relative to 2010–2020, the total 0–2,000 m stratification at 2090–2100

Table 1 | Observed and projected stratification changes in the global ocean

	N^2 (0–200 m)		N^2 (0–2,000 m)		N^2 (pycnocline)	
Units	$10^{-6}\,s^{-2}$	$\%\,dec^{-1}$	$10^{-6}\,s^{-2}$	$\%\,dec^{-1}$	$10^{-6}\,s^{-2}$	$\%\,dec^{-1}$
Observations (annual mean, 1960–2024)[a,b]	6.9±1.5	1.1±0.2	0.9±0.1	0.8±0.1	16.8±3.2	1.8±0.3
Observations (summer, 1960–2024)[a,b]	8.8±1.7	1.2±0.2	1.2±0.2	0.9±0.1	25.2±5.2	1.7±0.4
Observations (winter, 1960–2024)[a,b]	4.9±1.5	1.0±0.3	0.8±0.2	0.8±0.2	5.9±3.9	1.0±0.7
Projections (annual mean, SSP1-2.6, 2050–2060)[c,d]	3.9 [2.2,5.4]	1.0 [0.6,1.4]	0.9 [0.5,1.2]	1.2 [0.8,1.6]	8.6 [3.7,13.5]	1.0 [0.5,1.5]
Projections (annual mean, SSP2-4.5, 2050–2060)[c,d]	6.4 [4.5,8.5]	1.7 [1.2,2.1]	1.2 [0.9,1.5]	1.7 [1.2,2.1]	14.3 [7.9,20.3]	1.6 [1.1,2.1]
Projections (annual mean, SSP5-8.5, 2050–2060)[c,d]	9.5 [7.3,11.5]	2.3 [1.7,2.8]	1.7 [1.3,2.0]	2.3 [1.7,2.8]	20.0 [12.3, 29.6]	2.2 [1.5,3.1]
Projections (annual mean, SSP1-2.6, 2090–2100)[c,d]	2.9 [0.6,5.9]	0.4 [0.1,0.7]	1.0 [0.5,1.6]	0.7 [0.3,1.1]	7.1 [1.7,13.8]	0.4 [0.1,0.8]
Projections (annual mean, SSP2-4.5, 2090–2100)[c,d]	9.5 [6.4,12.1]	1.3 [0.9,1.5]	2.1 [1.4,2.7]	1.4 [0.9,1.8]	20.9 [10.8, 32.4]	1.2 [0.7,1.7]
Projections (annual mean, SSP5-8.5, 2090–2100)[c,d]	22.0 [15.2,29.9]	3.1 [2.2,4.1]	4.1 [2.7,5.3]	2.9 [2.1,3.8]	45.7 [27.5,68.8]	2.7 [1.8,3.7]
Projections (annual mean, SSP1-2.6, 2090–2100 minus 2050–2060)[d]	−1.0 [−2.0,−0.1]	−0.3 [−0.5,−0.0]	0.1 [−0.1,0.3]	0.1 [−0.2,0.5]	−1.5 [−3.3,0.6]	−0.2 [−0.4,0.1]
Projections (annual mean, SSP2-4.5, 2090–2100 minus 2050–2060)[d]	3.1 [1.5,4.4]	0.8 [0.4,1.1]	0.9 [0.5,1.2]	1.2 [0.7,1.6]	6.7 [2.8,11.2]	0.7 [0.4,1.2]
Projections (annual mean, SSP5-8.5, 2090–2100 minus 2050–2060)[d]	13.6 [9.0,18.7]	3.6 [2.5,5.0]	2.6 [1.7,3.4]	3.6 [2.5,4.8]	27.8 [14.0,40.9]	3.1 [1.7,4.4]

[a]Observational ocean stratification estimates are based on three datasets[55–57], with trends calculated by applying ordinary least squares regression to the ensemble-mean time series of the three datasets. For the summer and winter changes, only data from refs. 55,56 are used because of data availability. [b]90% confidence intervals for trends are given, whereby uncertainty is quantified by *t*-test analysis considering the reduction in degree of freedom. [c]Calculated as the difference relative to 2010–2020. [d]Model uncertainty is given for the 13–87% range.

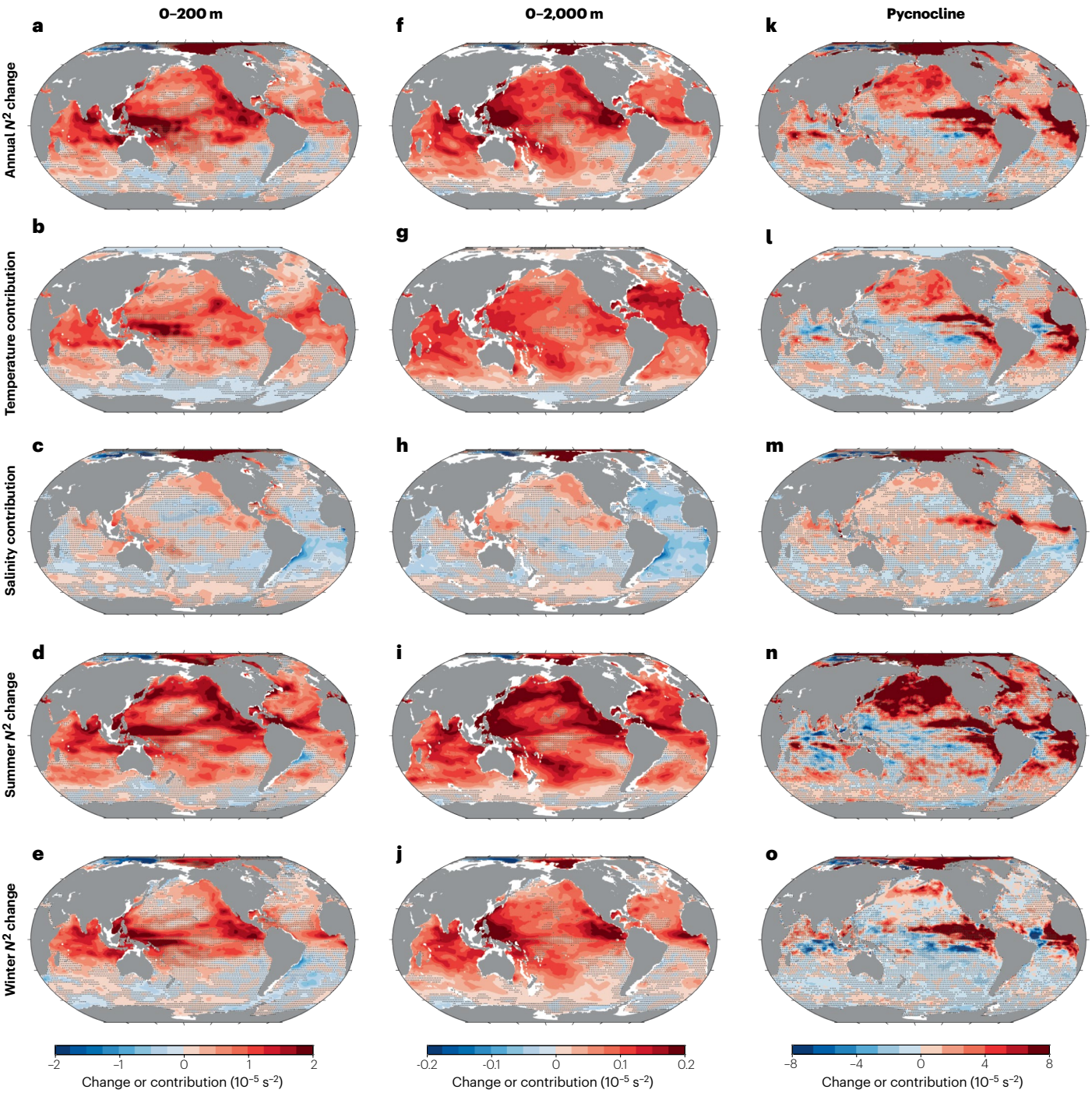

Fig. 4 | Observed regional stratification changes. a–**e**, Stratification changes and contributions[5] at 0–200 m depth over 1960–2024 from various observational products[54,56,57], including: the annual N^2 change (panel **a**), the contribution of temperature to the annual change (panel **b**, calculated as $N^2_\Theta = g\alpha^\Theta\Theta_z$), the contribution of salinity to the annual change (panel **c**, calculated as $N^2_{S_A} = -g\beta^\Theta S_{A_z}$), summertime changes (panel **d**; August–October in the Northern Hemisphere and January–March in the Southern Hemisphere) and wintertime changes (panel **e**; January–March in the Northern Hemisphere and August–October in the Southern Hemisphere). Stippling indicates regions with statistically insignificant changes at the 90% confidence level. **f**–**j**, As in panels **a**–**e** but for stratification changes and contributions at 0–2,000 m. **k**–**o**, As in panels **a**–**e** but for changes and contributions at the pycnocline. Note the different scales for the colour bars. Temperature and salinity changes contribute to observed regional ocean stratification changes, which feature strong seasonal differences.

is 1.4 [0.9,1.8]% dec^{-1} for SSP2-4.5 and 2.9 [2.1,3.8]% dec^{-1} for SSP5-8.5, ~2 and ~4 times the change for SSP1-2.6 (0.7 [0.3,1.1]% dec^{-1}) (Fig. 3b). This ongoing stratification reflects continuation of strong upper warming and moderate deep ocean warming up to 2100 (Fig. 3e,f and Supplementary Fig. 9). Diverging stratification responses post-2050 are also evident for 0–200 m and pycnocline definitions (Table 1 and Fig. 3a,c,d,f). Moreover, because these contrasting future projections under different scenarios are consistent with physical understanding of ocean responses, they are deemed to be robust.

Projected regional stratification changes

As in observations, enhanced stratification is a pervasive feature of the global oceans, albeit with temporal, scenario and seasonal variability. For SSP1-2.6, 94.0% of ocean grids (at 1° × 1°) exhibit enhanced 0–200 m stratification during 2050–2060 (Supplementary Fig. 10a), decreasing to 85.5% during 2090–2100 (Supplementary Fig. 10d). Yet, for SSP5-8.5, the area experiencing stratification increases remains fairly stable at 94.5% and 94.0% during the two time periods (Supplementary Fig. 10g,j). Most of these changes are associated with temperature (Fig. 5b,g and Supplementary Fig. 10), but as in observations, salinity is also regionally important[4] (Fig. 5c,h and Supplementary Fig. 10). For example, temperature change contributes 66.3% of the projected 0–200 m stratification increases (2.6 [1.2,4.5] × 10^{-6} s^{-2} or 0.7 [0.3,1.1]% dec^{-1}) during 2050–2060 and 38.8% (1.1 [−0.6,3.4] × 10^{-6} s^{-2} or 0.1 [−0.1,0.5]% dec^{-1}) during 2090–2100, respectively, under SSP1-2.6. For SSP5-8.5, however, thermal stratification dominates the projected 0–200 m stratification change, contributing 82.6% of the increase (7.8 [6.3,9.2] × 10^{-6} s^{-2} or 2.1 [1.7,2.5]% dec^{-1}) during 2050–2060 and 80.0% (17.6 [12.7,23.6] × 10^{-6} s^{-2} or 2.3 [1.7,3.1]% dec^{-1}) during 2090–2100, respectively. Likewise, regardless of the scenario, stratification differences are more pronounced in local summer than winter (Fig. 5d,e,i,j and Supplementary Figs. 10–13), consistent with the projected shallowing of mixed layer and amplified SST annual cycle[95,96]. These projections are consistent for the 0–2,000 m (Supplementary Figs. 11, 14) and pycnocline definitions (Supplementary Figs. 12, 15).

Strong regional variability in stratification projections and their contributions are also evident. The largest stratification increases in the upper 200 m are projected to occur in the tropical and subtropical regions (within 20° S to 20° N), especially in the Pacific (9.6 [5.7,16.0] × 10^{-6} s^{-2} or 0.7 [0.4,1.1]% dec^{-1} for SSP1-2.6, and 44.3 [31.5,60.1] × 10^{-6} s^{-2} or 3.3 [2.6,4.3]% dec^{-1} for SSP5-8.5) and Indian Oceans (7.8 [2.5,12.9] × 10^{-6} s^{-2} or 0.5 [0.2,0.9]% dec^{-1} for SSP1-2.6, and 36.0 [21.9,53.1] × 10^{-6} s^{-2} or 2.6 [1.8,3.6]% dec^{-1} for SSP5-8.5) within 2090–2100 relative to 2010–2020 (Fig. 5a,f). Temperature contributes most strongly to these changes in both scenarios, although signals are amplified by salinity change (Fig. 5b,c,g,h). For instance, an adjusted water cycle in tropical convection zones, manifesting as near-surface freshening[97], contributes to enhanced stratification. These changes are particularly apparent in the West Pacific and East Indian Warm Pool and ITCZ regions[97].

Stratification in the Arctic Ocean also experiences a sustained increase. Indeed, projected changes at 0–200 m are 2.1 [−6.6, 14.1] × 10^{-6} s^{-2} (0.8 [−0.8,2.1]% dec^{-1}) and 10.3 [−5.6,35.6] × 10^{-6} s^{-2} (2.1 [−0.7,6.3]% dec^{-1}) within 2090–2100 (relative to 2010–2020) for SSP1-2.6 and SSP5-8.5, respectively (Fig. 5a,f). This enhancement is probably contributed by salinity changes (Fig. 5c,h), where the loss of sea ice has a dominant role[98]. Contrasting surface and subsurface warming trend also have a role via increases in poleward heat transport[99]. However, substantial model biases in Arctic temperature and salinity[100–102] (Supplementary Figs. 10–12) mean that the relative contributions of temperature and salinity are uncertain in this location[103]. Similarly, the projected substantial stratification increase in the mid-latitude Atlantic Ocean related to salinity changes is likely to be a product of strong model salinity biases in this region[100,104].

Another consistent regional change is the projected decline in stratification in the subtropical gyres, especially in the Southeast Pacific and middle latitudes of the Atlantic Ocean (Fig. 5a,f). Different from other regions, there is no significant difference in magnitude of stratification changes in these regions between low-emission and high-emission scenarios, mainly because of the strong cancelling effects between temperature and salinity changes (Fig. 5b,c,g,h). Indeed, the salinity changes drive stratification decreases in the subtropical gyre regions, because the continuous increasing evaporation due to the water cycle amplification increases the near-surface salinity (Fig. 5c,h).

Consequences of long-term stratification changes

Observed and projected ocean stratification changes have substantial Earth system consequences. Amongst other facets, these include impacts on physical ocean attributes (ocean circulation, tides and mixing, marine heatwaves), biogeochemical ocean attributes (greenhouse gas fluxes, biogeochemical changes) and attributes that are more climatic (Earth surface warming, climate modes, tropical cyclones and tipping points), all of which are now discussed (Fig. 6).

Ocean heat uptake and surface warming

Ocean stratification influences the rate of global surface warming under greenhouse gas forcing[4,21,105]. Stronger stratification tends to be associated with enhanced surface layer warming relative to layers below the permanent pycnocline and, hence, lower efficiency of ocean heat uptake, through reduced vertical mixing[22,106] (Fig. 7a). Such near-surface intensified warming, in turn, further increases stratification, amplifying the impact on ocean heat uptake, reflecting a positive feedback. Regional stratification changes have different roles in surface temperature changes. For instance, surface salinification driven by the amplified water cycle reduces the upper-ocean stratification in subtropical oceans and therefore strengthens ocean heat uptake — a negative feedback to surface warming[21].

The strength of upper-ocean stratification is also important in determining the intensity of vertical mixing, which, in turn, affects the development of the mixed layer and the entrainment process at the base of the mixed layer. For example, in the Arabian Sea, enhanced near-surface stratification contributes to the increased radiative forcing-induced sea surface warming by inhibiting vertical mixing[107]. In the Arctic, upper-ocean stratification dominated by freshwater input shoals the mixed layer, limiting heat flux from the deeper ocean to the surface layer[84]. At the high latitudes of the Southern Ocean, surface freshening induced by meltwater and precipitation increases near-surface stratification, reducing convective overturning and the entrainment of relatively warm subsurface waters into the surface layer, cooling the ocean surface. These cooling signals enhance sea-ice coverage[108,109] and promote earlier sea-ice advance[110,111], with corresponding impacts on regional and remote surface temperature[112].

Future stratification changes exert a further impact on ocean heat uptake and surface temperature changes. These influences, however, depend on the relative importance of fast and slow ocean responses. In low-emission scenarios, upper-ocean stratification increases first, further enhancing surface warming. After ~2050–2060, stratification

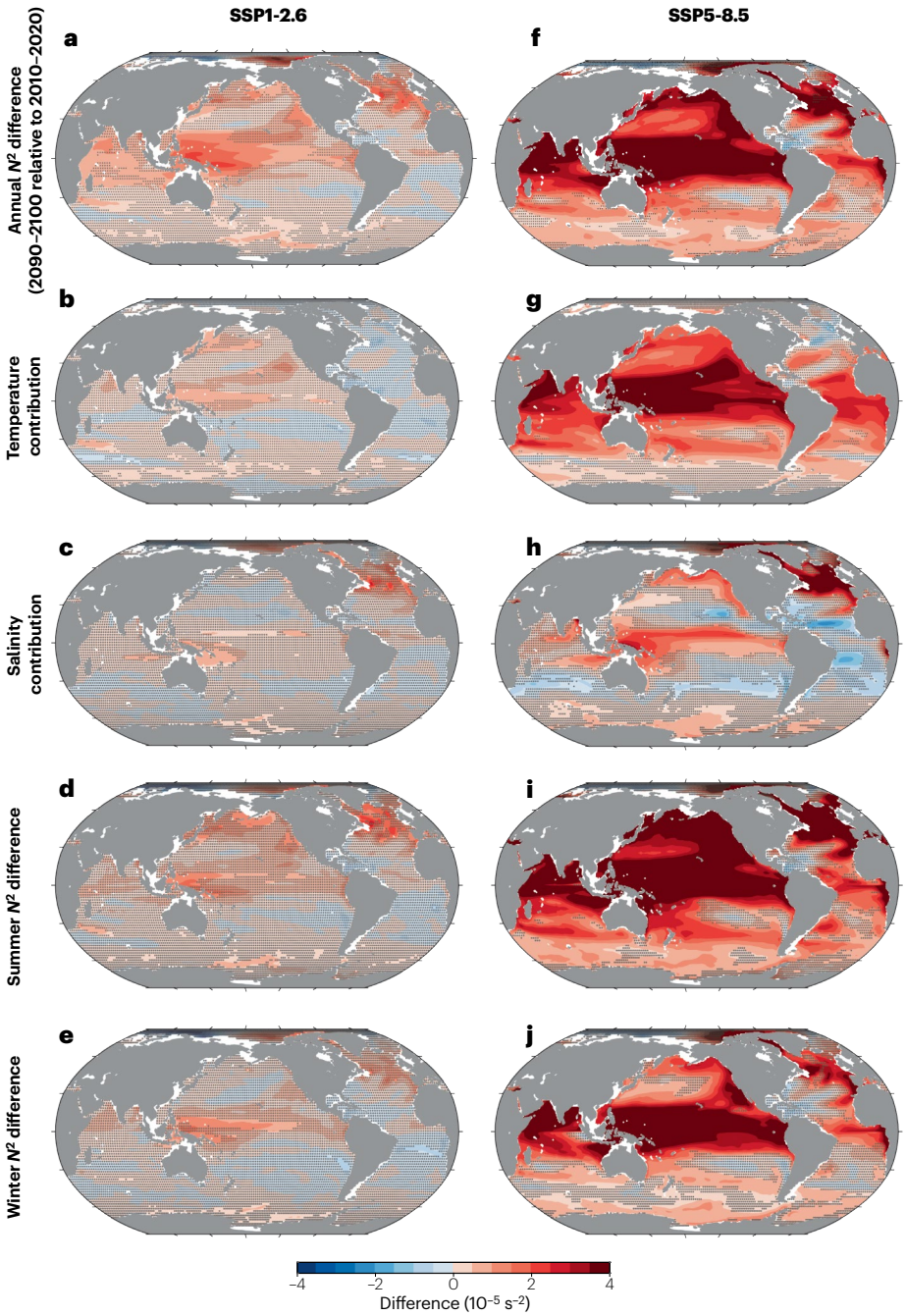

Fig. 5 | Future stratification change sensitivity to emission scenario. a–**e**, Ensemble-mean stratification changes for 0–200 m by 2090–2100 relative to 2010–2020 in CMIP6 models[90] forced with SSP1-2.6, including: the annual N^2 change (panel **a**), the contribution of temperature[5] to the annual change (panel **b**, calculated as $N^2{}_\Theta = g\alpha^\Theta\Theta_z$), the contribution of salinity[5] to the annual change (panel **c**, calculated as $N^2{}_{S_A} = -g\beta^\Theta S_{A_z}$), summertime changes (panel **d**; August–October in the Northern Hemisphere and January–March in the Southern Hemisphere) and wintertime changes (panel **e**; January–March in the Northern Hemisphere and August–October in the Southern Hemisphere). Stippling indicates where the multimodel mean anomaly is less than the intermodel standard deviation. **f**–**j**, As in panels **a**–**e** but for SSP5-8.5. Projected ocean stratification change is unevenly distributed, with future change dependent on socioeconomic scenarios.

gradually decreases owing to slow deep ocean warming and decreased greenhouse gas emissions, limiting temperature increases[94,113,114] (Fig. 3 and Supplementary Fig. 9). By contrast, in mid-emission or high-emission scenarios, stratification continues increasing throughout the twenty-first century, associated with an amplified effect on surface warming.

Stratification changes are strongly relevant to the occurrence and magnitude of marine heatwaves. Indeed, stratification is an important precondition for marine heatwaves[115–117], decreasing entrainment of cool water from below, and reducing the thickness of the surface layer that absorbs heat from the atmosphere, making the surface ocean easier to warm[116,118]. The expected future increase in stratification will therefore further increase the intensity and frequency of marine heatwaves, causing severe biological impacts, including mass mortality and habitat shifts[119–121]. These impacts could occur in ecosystems historically insulated from surface ocean heating by the cooling effects of internal waves[122].

However, weak ocean stratification can also have a detrimental effect on marine heatwaves. For example, in coastal waters off

southeastern Australia, weak ocean stratification allows wind-driven downwelling of warm water, extending the heatwave below the mixed later[115,123,124]. Such sub-mixed-layer marine heatwaves tend to last longer than surface heatwaves[124,125] owing to possible seasonal re-emergence of subsurface anomalies that drive multiyear events[116,118,126–128].

Ocean circulation

Vertical stratification changes crucially modulate ocean circulation responses in many regions[129,130]. For instance, enhanced vertical stratification causes shoaling of subtropical gyre depth, in turn, driving the spin-up of the subtropical upper circulation[129,131–135]. Similarly, the Equatorial Undercurrent intensifies as it shoals under stronger vertical stratification induced by surface warming[129,136]. In the Northwest Pacific, strengthened ocean stratification enhances eddy kinetic energy in the downstream Kuroshio extension region, intensifying the recirculation gyre to its south, further accelerating the Kuroshio extension[133]. Fast surface warming and corresponding enhanced ~200–400 m stratification also cause an onshore intensification of Western Boundary Currents[137] (Fig. 7b).

Yet many other circulation systems weaken because of stratification changes. For instance, strong freshening in the subpolar North Atlantic in a warmer climate enhances vertical stratification, reducing the formation of North Atlantic Deep Water and thus slowing the AMOC[132,138,139]. Indeed, with rising atmospheric CO_2 concentrations, AMOC periodicity and amplitude tend to decline, largely related to a more stratified subpolar North Atlantic that changes the characteristics of westward-propagated oceanic baroclinic Rossby waves[140,141]. The weakened AMOC decelerates the Gulf Stream[138] and remotely reduces the Indonesian Throughflow transport through interbasin Kelvin-wave propagation along the coastal-equatorial waveguide[114,132]. Although stratification in the North Atlantic is pivotal, palaeoclimate evidence indicates that AMOC stability during the last deglaciation is mostly determined by salinity stratification at ~34° S (refs. 142,143) (Fig. 7c).

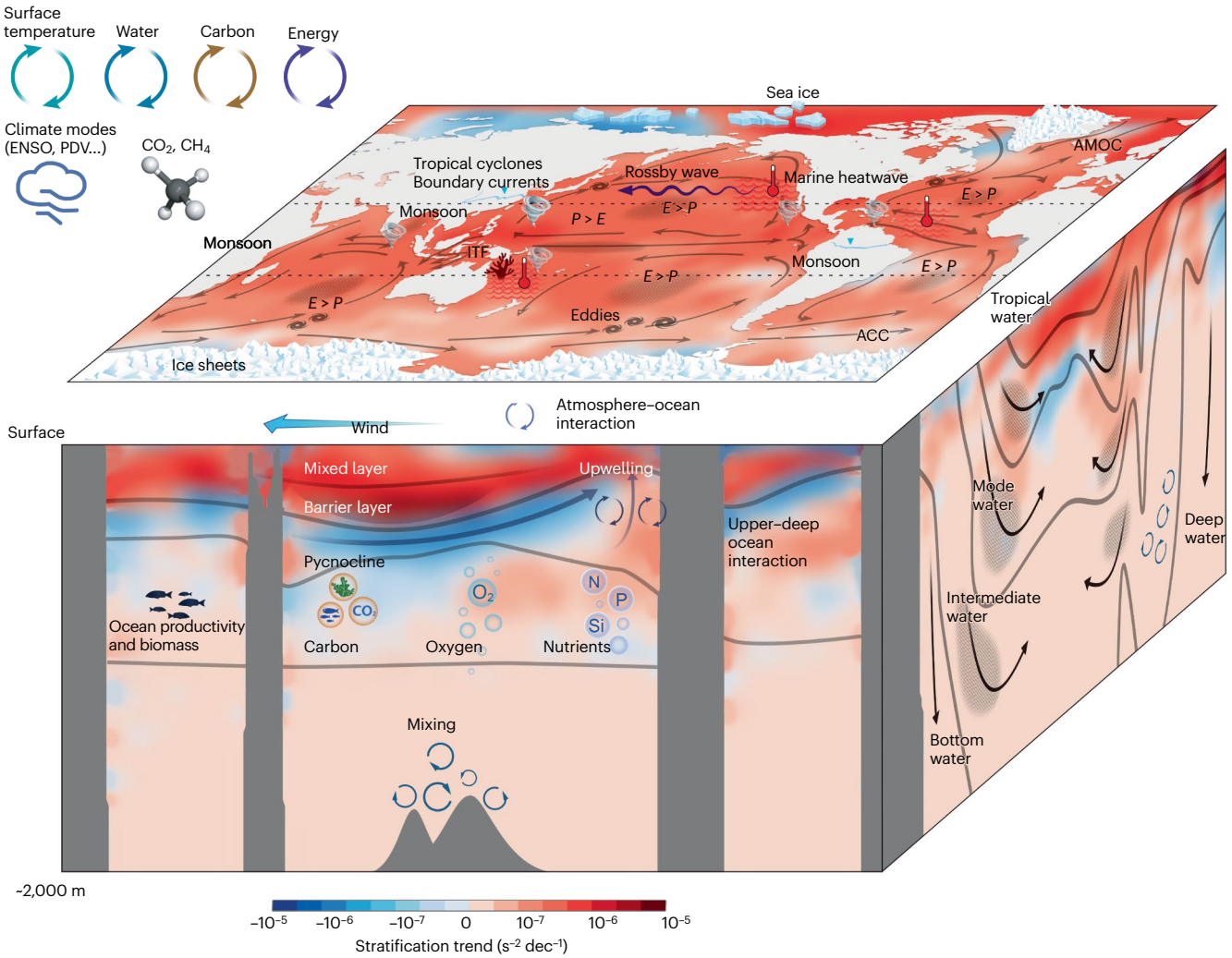

Fig. 6 | Ocean stratification impacts on physical and biogeochemical ocean systems. The observed[5] mean N^2 trend for 0–2,000 m (upper), meridional N^2 trend within 20° S to 20° N (front), and zonal mean N^2 trend (right), with icons demonstrating their importance in the global climate system. Ocean stratification change is a pervasive feature and has important impacts on the climate system. ACC, Antarctic Circumpolar Current; AMOC, Atlantic Meridional Overturning Circulation; *E*, evaporation; ENSO, El Niño–Southern Oscillation; ITF, Indonesian Throughflow; *P*, precipitation; PDV, Pacific Decadal Variability.

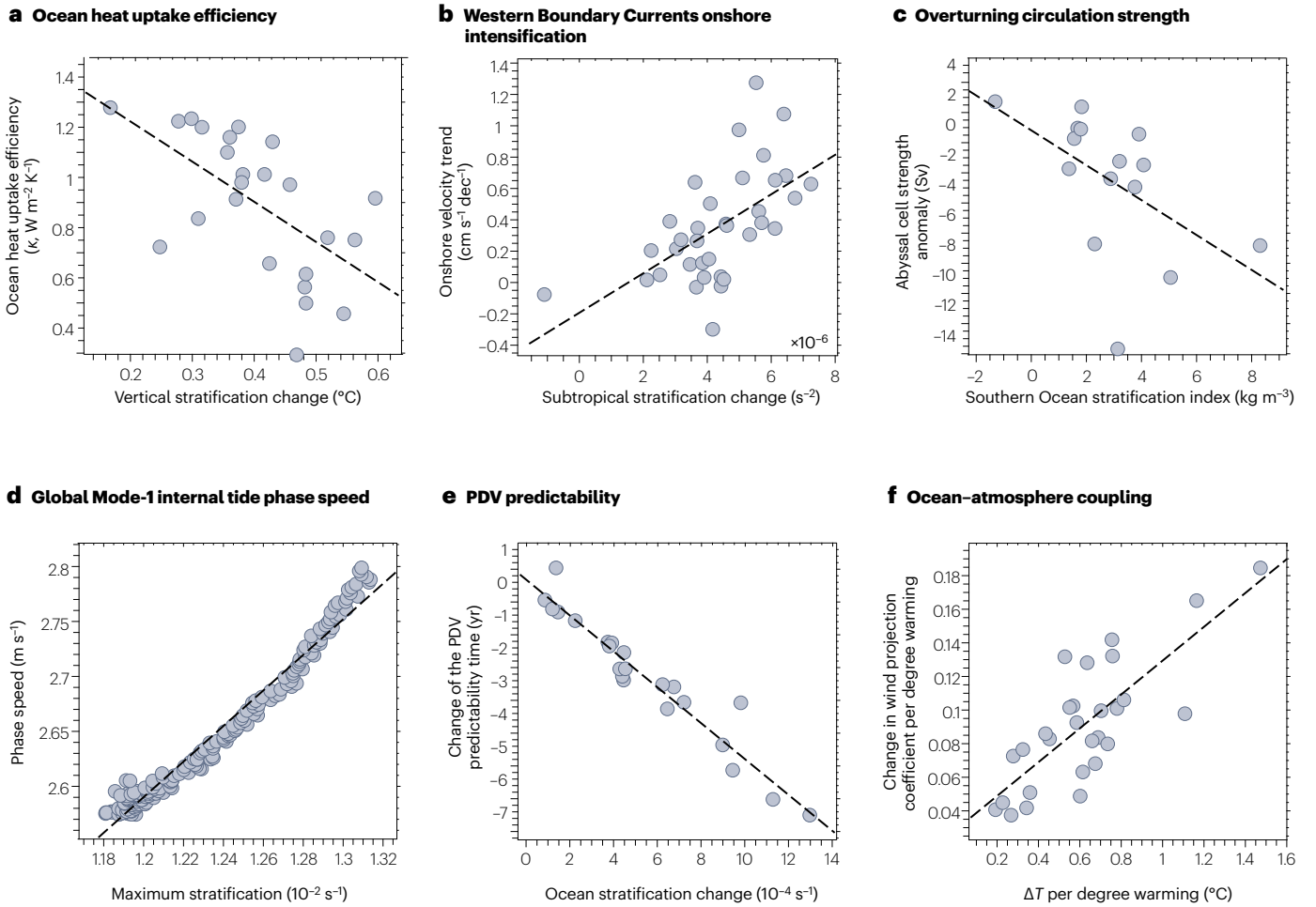

Fig. 7 | Quantifying the impact of stratification on the climate system. **a**, Intermodel relationship between ocean heat uptake efficiency (κ) and globally averaged vertical stratification change (the temperature difference between 0–100 m and 1,500–2,000 m) in CMIP6 historical simulations[90] from 1900 to 2014; as in ref. 22. **b**, Intermodel relationship between onshore velocity trends of Western Boundary Currents and changes in oceanic stratification averaged between 200–400 m in five subtropical basins (both representing the difference between 2015–2050 (SSP5-8.5) and the 1950–2014 (historical simulation) periods, scaled by the global-mean sea surface temperature difference between the projected mean and the historical mean) in seven CMIP6 models; as in ref. 137. **c**, Intermodel relationship between the Atlantic Meridional Overturning Circulation (AMOC) abyssal cell strength anomalies (defined as the absolute value of the most negative global meridional overturning stream function below a depth of 1,000 m) and the Southern Ocean stratification index (defined as $SI = \sum\rho(z_i) - \rho(z_0)$, where z_0 is the sea surface and $z_i = z_{i-1} + 200$ for $i = 1,\ldots,10$, at upper 2,000 m Southern Ocean within 45° S to -90° S). The AMOC anomalies are the difference between the mid-Pliocene warm period and preindustrial period in the second phase of Pliocene Model Intercomparison Project (PlioMIP2) simulations[143]. **d**, Relationship between global-averaged Mode-1 internal tide phase speed (c_{p1}) via solving the Taylor–Goldstein equation, and the maximum vertical buoyancy frequency (N) in CMIP6 simulations from 1901 to 2100 for historical and SSP1-2.6, SSP2-4.5, SSP3-7.0 and SSP5-8.5 simulations (each dot is one year); as in ref. 155. **e**, Intermodel relationship between changes in the predictability time of the Pacific Decadal Variability (PDV, defined as a lead time when the PDV can be predicted at a certain confidence level, with negative anomalies indicating reduced predictability) and changes in ocean stratification (the mean N^2 of the upper 400 m ocean averaged over the North Pacific sector, 30–60° N, 120° E–140° W) in CMIP5 simulations, with change representing the difference between Representative Concentration Pathways (RCP2.6, RCP4.5 and RCP8.5) from 2006–2099 and the PiControl (last 294 years of each model); after ref. 205. **f**, Intermodel relationship between the wind–ocean coupling (quantified by a wind projection coefficient associated with the first three baroclinic modes to characterize the mean thermocline shape, depth and intensity) and changes in equatorial ocean stratification (the difference between the mean temperature over the upper 75 m and the temperature at 100 m averaged over 150° E to 140° W) in historical and RCP8.5 simulations of CMIP5 models, with values representing anomalies between future (2000–2099) and present-day (1900–1999) climates; as in ref. 211. The dashed lines represent linear regression. Ocean stratification and its change intervene in the dynamics of ocean and air–sea interaction, and thus become a controlling factor of the future climate responses.

Thus, this enhanced stratification in the Southern Ocean would reduce Antarctic Deep Water formation and, in turn, reduce anthropogenic ocean CO_2 uptake[143,144].

Additionally, enhanced vertical stratification decelerates deep ocean currents. Strengthened stratification with warming decreases the available potential energy stored in the large-scale ocean

circulation, reducing its conversion into eddy kinetic energy and leading to a more quiescent deep ocean[145]. Sensitivity experiments reveal that enhanced vertical stratification increases upper-ocean circulation but systematically decreases deep ocean currents[146].

Surface and internal tides

Barotropic surface tides (the rise and fall of sea levels caused by gravitational forces exerted by the Moon and Sun) and internal tides (generated by barotropic tidal currents flowing over rough topographic features) are both altered by increasing stratification. These tide changes directly influence interior ocean mixing[147,148], thereby affecting vertical heat, freshwater and carbon exchanges.

Enhanced stratification influences barotropic tides differently in the open ocean and marginal seas. For example, observed stratification increases are believed to have caused a −0.1 to −0.5 mm yr^{-1} decline in global open-ocean barotropic M_2 tidal amplitudes during 1993–2020 (refs. 70,149–152). In shallow marginal seas, by contrast, stratification increases can enhance barotropic tides. In the East China and Yellow Seas[153], surface-warming-related thermal stratification stabilizes barotropic rotary flows through turbulent dissipation; such hydrodynamic stabilization manifests as positive M_2 tidal amplitude trends of 1.0–1.5 mm yr^{-1} (refs. 149,154). Complementary amplification mechanisms operate in estuarine systems, where pronounced haline stratification diminishes the bottom drag effect, thereby enhancing local barotropic tidal amplitudes[154].

In contrast to the reduced open-ocean surface tides, internal tides have generally increased as a result of stratification. Specifically, internal tidal-induced surface height has strengthened by ~6% since 1995 (ref. 151), a change that is expected to increase into the future; under SSP5-8.5, internal tide generation and propagation speed is projected to increase 8% and 10%, respectively, by the end of the twenty-first century[70,148,150,155]. These changes are associated with enhanced permanent pycnocline stratification; the increased vertical density gradient strengthens conversion rates from barotropic tidal energy to internal tidal energy at generation sites[148], and accelerates phase speeds of constant-frequency internal tides following the dispersion relationship[155] (Fig. 7d). The enhanced and accelerated internal tides predominantly break near their generation sites, elevating globally averaged mixing by ~6%[148]. However, pronounced regional differences emerge in internal tide responses to a warming climate. For example, in the Luzon Strait, intensified upper-ocean stratification causes the thermocline to shoal and become more stable, reducing energy conversion efficiency and leading to a 22.7% decline in internal tide generation under SSP5-8.5 (ref. 156). In contrast, in the Andaman Sea, increasing stratification deepens and sharpens the pycnocline, facilitating more effective barotropic-to-baroclinic energy conversion, and resulting in an 8% increase in internal tide generation[157]. These contrasting responses primarily stem from how regionally varying oceanographic conditions modulate the impact of enhanced stratification on internal tide generation and dissipation. In turn, the changing internal tide dissipation could also influence ocean stratification via interior mixing.

Biogeochemical and biological impacts

Stratification impacts the ocean's carbonate system and physical and biological carbon pumps, modulating climate change through interlinked and nonlinear feedbacks[158]. Increased upper-ocean stratification reduces the transport of anthropogenic dissolved inorganic carbon from the mixed layer into the ocean's deeper layers and, hence, anthropogenic CO_2 uptake[27]. Indeed, in combination with circulation changes, stratification is believed to have reduced the oceanic sink of anthropogenic carbon by 15% over 1994–2004 and 25% over 2004–2014 (ref. 23). By contrast, rainfall can enhance ocean carbon uptake by changing near-surface ocean turbulence associated with stratification and winds, modulating the air–sea CO_2 concentration gradient[159–161].

Ocean stratification also modifies the biological pump through effects on primary production and ocean biomass[25,162]. Increased near-surface stratification reduces mixing, providing improved light availability for photosynthesis[163]. These effects are particularly important in the high latitudes where phytoplankton are typically light limited. However, reduced mixing also decreases nutrient fluxes from the deep into the euphotic zone, enhancing nutrient limitations[164–166] and causing broad declines in net primary production[92,167,168]. These nutrient limitations are particularly apparent in tropical and mid-latitude oceans, where phytoplankton nutrient stress is already worsened under anthropogenic warming[165]. Overall, the joint effects from enhanced ocean stratification and changes in light, nutrients, grazing and SST are projected to decrease tropical net primary production by 7–16% by 2100 (refs. 17,169,170) and global net primary production by 3.0–8.5% depending on the scenario[171], highlighting decreased efficiency of the biological pump in sequestering atmospheric CO_2 (ref. 172). These changes will have knock-on effects on ocean biomass and diversity, including declines in fisheries catch[17,173–175].

Methane (CH_4) is also affected. Marine CH_4 emissions are from two main sources[176]: sediments at the sea floor and organic matter cycling in seawater[177]. In coastal or shallow seas, CH_4 from sediments can reach the atmosphere through the stratified ocean directly via bubbles or indirectly via vertical turbulent transport[178,179]. Thus, increased stratification inhibits the penetration of dissolved gases into the near-surface layer and hampers CH_4 fluxes to the atmosphere. Ocean temperature changes at the bottom affect the stability of methane clathrates, and possibly encourage methane release from marine sediments[177,180]. Also, ocean warming and upper-ocean stratification change affect CH_4 through phytoplankton growth, zooplankton egestion and other processes[179].

Stratification further strongly influences ocean oxygen content. Indeed, it is a key driver of ocean deoxygenation[27,171,181], contributing to the observed ~0.5–2% decline of global open-ocean dissolved oxygen from 1970 to 2010 (ref. 17). Thus, stratification prevents equilibration of the ocean interior with the atmosphere[166,182]. Stratification impacts on deoxygenation are also apparent regionally. In the Arabian Sea, for example, upper-ocean stratification increases linked to fast surface warming suppress ventilation of the intermediate ocean, exacerbating suboxic conditions; over 1982–2010, ocean oxygen inventories north of 20° N dropped by 6% dec^{-1} in the 100–1,000 m layer[183]. Salinity stratification also has a role in some locations. For example, upper-ocean salinification in the subtropical Atlantic Ocean weakens upper stratification, increasing ventilation of mode waters and thus subsurface oxygen content, opposing warming-driven oxygen loss[184]. By contrast, in the subpolar Atlantic Ocean, upper-ocean freshening increases upper stratification, reducing ventilation of deep waters to accelerate oxygen loss[184].

Tropical cyclone intensity

Tropical cyclone development is critically sensitive to underlying ocean conditions governed by stratification. Indeed, upper-ocean stratification determines the efficiency of colder subsurface waters being entrained to the surface and air–sea interaction strength, in

combination with other upper ocean characteristics, such as mixed-layer depth and mesoscale eddies[185–187]. These processes are critical for the intensity of the tropical cyclones.

Stratification can either amplify or subdue tropical cyclone intensification[68]. For example, rising SST and ocean heat content associated with enhanced stratification will provide more energy to the cyclones[186,188]. Increased stratification also inhibits diapycnal mixing and reduces cyclone-induced surface cooling (cold wake)[189]. Upper-ocean freshening caused by rainfall can also further intensify tropical cyclones by increasing upper-ocean salinity stratification, which acts to suppress cyclone-induced surface cooling[190,191]. This effect is even pronounced when there is a freshwater-induced (rainfall or river systems) barrier layer[190], by increasing ocean stability and suppressing storm-induced vertical mixing and cold wake. Thus, in a warming world with enhanced stratification, these effects would cause an increase in cyclone intensity[192], as already apparent in observations[192–194], albeit with uncertainty.

However, stratification can also reduce cyclone intensification. For instance, if tropical cyclone mixing is large enough to break through the warm, upper stratified layer, a stronger cold wake[195–198] would decrease surface enthalpy flux, reducing cyclone intensity and inner-core rainfall[68,195,196,199]. Moreover, internal tides can interact with cyclone-generated oceanic near-inertial waves, and can amplify mixing, weakening local stratification and causing strong ocean cooling, suppressing tropical cyclone intensification[200]; these effects are observed in the South China Sea. All in all, the net effects of stratification on tropical cyclones are sensitive to location and still debated.

Climate modes

Stratification changes also affect decadal modes of climate variability such as PDV. This relationship occurs through stratification-related impacts on Rossby-wave speed[201]; the stronger the stratification, the faster the Rossby-wave propagation[202]. The westward propagation of the Rossby wave is a key process setting the decadal timescale of the PDV, associated with the integration along Rossby-wave trajectories of stochastic forcing due to internal atmospheric dynamics[203,204]. Increased stratification therefore acts to reduce the PDV lifespan through faster propagation of extratropical oceanic Rossby waves in the Pacific[141,205]. The faster propagation of Rossby waves also corresponds to a shortened growth time, so the PDV amplitude is suppressed[205]. Accordingly, predictability of the PDV is reduced in a warming climate with stronger stratification, as the dynamics of the Rossby-wave propagation is the primary memory of PDV[205]. The consequence is a less-predictable global decadal climate variability in the future, because PDV is a primary climate variability on decadal timescale, which substantially affects global-mean surface temperature and regional climate[206,207] (Fig. 7e).

In addition to PDV, stratification changes also have bearing on ENSO. Generally, strong stratification favours an increase in air–sea coupling strength (Fig. 7f) through enhanced intensity of the thermocline response, because for the same atmospheric forcing the ocean baroclinic modes trap more momentum[208–210]. These interactions affect ENSO-related SST variability[211], driving increased frequency of extreme El Niño[212], extreme La Niña events[213] and consecutive ENSO events[214–216] in the future. Conversely, increased upper-ocean thermal stratification inhibits thermocline depth variations and nonlinear SST responses, lowering the amplitude of weaker events[217]. As with the PDV, stratification-related impacts on ocean wave propagation also contribute to more rapid development and decay of ENSO events in a warming climate[218]. These mechanisms also apply in the Indian Ocean, potentially increasing Indian Ocean Dipole variability in the twenty-first century for warming levels higher than 1.5 °C (refs. 219,220). However, as current generation models have limited capability in simulating the mean state and variations of the tropical ocean[221,222], stratification influences on modes of variability are uncertain.

Tipping points and abrupt changes

The change in ocean stratification is considered to be critical to several tipping points in the climate system; slow changes in one Earth system component pass a tipping point, after which impacts cascade through coupled climate–ecological–social systems[25,223,224]. Stratification could hypothetically be relevant to two tipping points — the AMOC, and Antarctic sea ice — although the connections are currently speculative.

A key tipping point is the collapse of AMOC. Under high greenhouse gas emission scenarios, warming and freshening could cause convection in the Labrador Sea to collapse[225,226]. This density-related collapse could lead to a shutdown in the AMOC, with accompanying abrupt changes in regional climate regimes[227,228]. Although models consistently project moderate changes in AMOC under future warming scenarios, some suggest that model biases favouring an overly stable AMOC might lead to an underestimation of the prospects for AMOC weakening or shutdown[229]. Palaeoclimate data spanning the past millennium hint at this possibility as well[230].

An additional possible tipping point is focused on the Antarctic. Palaeoclimate records indicate bimodal switches associated with a feedback between sea ice and ocean deep convection[231]. Strong convection brings warm water to the surface (weak stratification), preventing sea ice from forming, allowing cooling of surface water and favouring convection. Meanwhile, sea-ice formation and resultant brine rejection reduce stratification, in turn, inhibiting the formation of sea ice[232]. Furthermore, when the sea surface is covered by perennial sea ice, much less brine formation occurs, favouring strong stratification and enabling the formation of more sea ice[232]. Through these feedback loops, stratification changes could potentially trigger abrupt Southern Ocean changes.

Summary and future perspectives

Ocean stratification is an important oceanic process with substantial climatic implications. Robust stratification increases have been observed since the 1960s, with rates of 1.1 ± 0.2% dec^{-1}, 0.8 ± 0.1% dec^{-1} and 1.8 ± 0.3% dec^{-1} for 0–200 m, 0–2,000 m and seasonal pycnocline stratification, respectively (Table 1 and Fig. 3); temperature contributes most strongly to these changes, but salinity can be important regionally. These increases are most prominent in the tropics and during summer. Although climate models suffer from uncertainties and biases, they project the increased stratification trend will continue (Fig. 3). However, the magnitude of ongoing changes depends strongly on the emission scenario and the timescale considered (Table 1 and Figs. 3, 5): under a low-emission scenario (SSP1-2.6), 0–2,000 m stratification increases up to ~2050–2060 (1.2 [0.8,1.6]% dec^{-1} relative to 2010–2020) and stabilizes up to 2100 (0.7 [0.3,1.1]% dec^{-1} relative to 2010–2020), whereas for moderate and high-emission scenarios, it increases up to ~2050–2060 (1.7 [1.2,2.1]% dec^{-1} and 2.3 [1.7,2.8]% dec^{-1} for SSP2-4.5 and SSP5-8.5, respectively, relative to 2010–2020) and continues to 2100 (1.4 [0.9,1.8]% dec^{-1} and 2.9 [2.1,3.8]% dec^{-1} for SSP2-4.5 and SSP5-8.5, respectively, relative to 2010–2020). This divergence has important implications for future climate changes owing to the different strengths of atmosphere–ocean and upper–deep ocean interactions (Figs. 6,7). However, further research is needed to better monitor,

understand, simulate and project the changes in ocean stratification, as now discussed.

Quantification of trends is sensitive to the definition of stratification, leading to potential confusion. As ocean stratification changes vary with depth, trends cannot be defined solely by characteristics in one layer. For instance, the density gradient in the 15-m layer directly below the mixed-layer base primarily defines seasonal pycnocline stratification. Moreover, the different definitions represent different dynamic regimes and, hence, might be relevant for some applications compared with others. For example, stratification changes in the mixed layer and seasonal pycnocline are relevant to tropical cyclones and ocean production, whereas stratification changes in the permanent pycnocline would be more relevant to effects on wind-driven circulation, internal tides and climate modes. Hence, there is no single 'best' definition: the stratification layer always needs to be specified and justified according to the relevance and dynamic considerations.

Stratification changes at or near critical layers need to be better quantified and understood. These critical layers include the seasonal and permanent pycnocline, as well as the mixed layer and barrier layer, where substantial uncertainty exists[3,5,6] owing to data limitations. To better quantify these changes, efforts are needed to understand underlying data quality and methodologies, including the impact of temporal and spatial coverage, gap-filling and regression approaches; and to develop methodologies to better detect the critical ocean layers such as the pycnocline in middle and high latitudes. As stratification is defined as the vertical gradient of ocean density, the observational requirements are different for temperature and salinity[233,234]. Thus, the capability of the current observation system to quantify stratification changes should also be evaluated.

In addition to improved observational systems, model development and evaluation of ocean stratification is needed, highlighting immediate priorities. Current-generation climate models contain substantial biases that will affect the simulation of stratification and thereby their projected trends. Important biases include SST[235–237] and its change patterns[238,239], subsurface temperatures[12] and salinity[100,240], and mixing and diffusion[241]; the latter should be key targets to better represent the vertical structure of ocean properties and ocean circulations. In particular, climate models exhibit a large spread in projecting ocean heat uptake efficiency[22,106,242], primarily driven by the intermodel spread of the middle-latitude ventilation associated with the (permanent) pycnocline depth[242], and also parameterization of vertical mixing and diffusivity[22,243]. Therefore, constraining the model spread in middle-latitude stratification by observations could help to constrain the uncertainty in future projections of anthropogenic carbon uptake[244] and heat uptake[106,245].

Beyond models, palaeo-observations of stratification changes also hold promise but have not been examined in detail. Regional proxy data indicate a strong stratification in the deep ocean (cold and salty water) during the Last Glacial Maximum (~21,000 years ago), leading to an elevated oceanic carbon storage during this period and subsequent release during the deglaciation when stratification decreased[246,247]. During the Holocene (beginning ~11,700 years ago), stronger upper-ocean stratification in the tropical East Pacific favours more multiyear ENSO events during that period because of more efficient ocean–atmosphere coupling[216]. These investigations suggest a crucial role of stratification in palaeoclimate changes. Thus, linking modern climate observations with palaeoclimate provides could offer critical insight into climate system responses in the current and future climate. Doing so requires integrating all available proxy records, and developing more proxy records over the world's ocean, to better resolve the vertical structure of stratification changes before the middle of the twentieth century.

Although it is well accepted that ocean stratification has increased, fundamental questions about the causes and impacts of these changes remain. For instance, attribution of stratification changes is lacking, necessitating investigations into the key mechanisms (winds, buoyancy or ocean dynamics) and drivers (greenhouse gases, aerosols or climate variability) at global and regional scales. Dedicated model-based analyses with single-forcing experiments (after properly accounting for model biases in stratification) could contribute understanding. Moreover, the impact of these stratification changes, particularly on ecosystems and society, needs to be better quantified. Ocean stratification is established as a crucial driver of deoxygenation, but the magnitude of the contribution is little known[182]. Likewise, influences on primary production, ocean biomass and the carbon cycle have not been well quantified, nor have the compound effects of stratification increases together with other ocean changes (such as warming, acidification and deoxygenation). Finally, isolating the impacts of stratification from other factors and phenomena is challenging – stratification is not an independent variable. For example, the positive and negative feedbacks of stratification change on tropical cyclones are mixed with temperature and salinity effects, meaning that the direct net impact cannot be quantified. New analysis approaches should be developed to clarify these effects, including model experiments and theoretical analyses linked to observations.

Published online: 30 September 2025

References

1. Sprintall, J., Cronin, M. & Farrar, J. T. in *Encyclopedia of Ocean Sciences* Vol. 1 (eds Cochran, J. K., Bokuniewicz, H. J. & Yager, P. L.) 97–105 (Elsevier, 2010).
2. Ivey, G. N., Winters, K. B. & Koseff, J. R. Density stratification, turbulence, but how much mixing? *Annu. Rev. Fluid Mech.* **40**, 169–184 (2008).
3. Yamaguchi, R. & Suga, T. Trend and variability in global upper-ocean stratification since the 1960s. *J. Geophys. Res. Oceans* **124**, 8933–8948 (2019).
4. Capotondi, A., Alexander, M. A., Bond, N. A., Curchitser, E. N. & Scott, J. D. Enhanced upper ocean stratification with climate change in the CMIP3 models. *J. Geophys. Res. Oceans* **117**, C04031 (2012).
5. Li, G. et al. Increasing ocean stratification over the past half-century. *Nat. Clim. Change* **10**, 1116–1123 (2020).
6. Sallée, J.-B. et al. Summertime increases in upper-ocean stratification and mixed-layer depth. *Nature* **591**, 592–598 (2021).
7. Yamaguchi, R., Suga, T., Richards, K. J. & Qiu, B. Diagnosing the development of seasonal stratification using the potential energy anomaly in the North Pacific. *Clim. Dyn.* **53**, 4667–4681 (2019).
8. Peng, S. & Wang, Q. Fast enhancement of the stratification in the Indian Ocean over the past 20 years. *J. Clim.* **37**, 2231–2245 (2024).
9. Simpson, J. H. et al. The shelf-sea fronts: implications of their existence and behaviour. *Phil. Trans. R. Soc. A* **302**, 531–546 (1981).
10. Somavilla, R., González-Pola, C. & Fernández-Diaz, J. The warmer the ocean surface, the shallower the mixed layer. How much of this is true? *J. Geophys. Res. Oceans* **122**, 7698–7716 (2017).
11. Rhein, M. et al. in *Climate Change 2013: The Physical Science Basis* (eds Stocker, T. F. et al.) Ch. 3 (IPCC, Cambridge Univ. Press, 2013).
12. Cheng, L. et al. Past and future ocean warming. *Nat. Rev. Earth Environ.* **3**, 776–794 (2022).
13. Gulev, S. et al. in *Climate Change 2021: The Physical Science Basis* (eds Masson-Delmotte, V. et al.) Ch. 2 (IPCC, Cambridge Univ. Press, 2021).
14. Cheng, L. et al. Improved estimates of changes in upper ocean salinity and the hydrological cycle. *J. Clim.* **33**, 10357–10381 (2020).
15. Durack, P. J., Wijffels, S. E. & Matear, R. J. Ocean salinities reveal strong global water cycle intensification during 1950 to 2000. *Science* **336**, 455–458 (2012).
16. Held, I. M. & Soden, B. J. Robust responses of the hydrological cycle to global warming. *J. Clim.* **19**, 5686–5699 (2006).
17. Bindoff, N. L. et al. in *Special Report on the Ocean and Cryosphere in a Changing Climate* (eds Pörtner, H.-O. et al.) 447–587 (IPCC, Cambridge Univ. Press, 2019).
18. Fox-Kemper, B. et al. in *Climate Change 2021: The Physical Science Basis* (eds Masson-Delmotte, V. et al.) Ch. 9 (IPCC, Cambridge Univ. Press, 2021).
19. Solomon, S., Plattner, G.-K., Knutti, R. & Friedlingstein, P. Irreversible climate change due to carbon dioxide emissions. *Proc. Natl Acad. Sci. USA* **106**, 1704–1709 (2009).

20. Abram, N. et al. in *IPCC Special Report on the Ocean and Cryosphere in a Changing Climate* (eds Pörtner, H.-O. et al.) 73–129 (IPCC, Cambridge Univ. Press, 2019).
21. Liu, M., Vecchi, G., Soden, B., Yang, W. & Zhang, B. Enhanced hydrological cycle increases ocean heat uptake and moderates transient climate change. *Nat. Clim. Change* **11**, 848–853 (2021).
22. Kuhlbrodt, T. & Gregory, J. M. Ocean heat uptake and its consequences for the magnitude of sea level rise and climate change. *Geophys. Res. Lett.* **39**, L18608 (2012).
23. Müller, J. D. et al. Decadal trends in the oceanic storage of anthropogenic carbon from 1994 to 2014. *AGU Adv.* **4**, e2023AV000875 (2023).
24. Schlunegger, S. et al. Emergence of anthropogenic signals in the ocean carbon cycle. *Nat. Clim. Change* **9**, 719–725 (2019).
25. Moore, J. K. et al. Sustained climate warming drives declining marine biological productivity. *Science* **359**, 1139–1143 (2018).
26. Breitburg, D. et al. Declining oxygen in the global ocean and coastal waters. *Science* **359**, eaam7240 (2018).
27. Gruber, N. Warming up, turning sour, losing breath: ocean biogeochemistry under global change. *Phil. Trans. R. Soc. A* **369**, 1980–1996 (2011).
28. Oschlies, A., Brandt, P., Stramma, L. & Schmidtko, S. Drivers and mechanisms of ocean deoxygenation. *Nat. Geosci.* **11**, 467–473 (2018).
29. Zhou, Y., Gong, H. & Zhou, F. Responses of horizontally expanding oceanic oxygen minimum zones to climate change based on observations. *Geophys. Res. Lett.* **49**, e2022GL097724 (2022).
30. Levin, L. A. Manifestation, drivers, and emergence of open ocean deoxygenation. *Annu. Rev. Mar. Sci.* **10**, 229–260 (2018).
31. Babbin, A. R., Bianchi, D., Jayakumar, A. & Ward, B. B. Rapid nitrous oxide cycling in the suboxic ocean. *Science* **348**, 1127–1129 (2015).
32. Suarez, M. J. & Schopf, P. S. A delayed action oscillator for ENSO. *J. Atmos. Sci.* **45**, 3283–3287 (1988).
33. Bjerknes, J. Atmospheric teleconnections from the equatorial Pacific. *Mon. Weather Rev.* **97**, 163–172 (1969).
34. Kim, S. T., Cai, W., Jin, F.-F. & Yu, J.-Y. ENSO stability in coupled climate models and its association with mean state. *Clim. Dyn.* **42**, 3313–3321 (2014).
35. Lukas, R. & Lindstrom, E. The mixed layer of the western equatorial Pacific Ocean. *J. Geophys. Res. Oceans* **96**, 3343–3357 (1991).
36. Liu, H., Grodsky, S. A. & Carton, J. A. Observed subseasonal variability of oceanic barrier and compensated layers. *J. Clim.* **22**, 6104–6119 (2009).
37. George, J. V. et al. Mechanisms of barrier layer formation and erosion from in situ observations in the Bay of Bengal. *J. Phys. Oceanogr.* **49**, 1183–1200 (2019).
38. Liang, Y.-C. et al. Amplified seasonal cycle in hydroclimate over the Amazon river basin and its plume region. *Nat. Commun.* **11**, 4390 (2020).
39. Sprintall, J. & Tomczak, M. Evidence of the barrier layer in the surface layer of the tropics. *J. Geophys. Res. Oceans* **97**, 7305–7316 (1992).
40. Maes, C., Picaut, J. & Belamari, S. Importance of the salinity barrier layer for the buildup of El Niño. *J. Clim.* **18**, 104–118 (2005).
41. Maes, C. & O'Kane, T. J. Seasonal variations of the upper ocean salinity stratification in the tropics. *J. Geophys. Res. Oceans* **119**, 1706–1722 (2014).
42. Liu, L., Huang, R. X. & Wang, F. Ventilation of a monsoon-dominated ocean: subduction and obduction in the north Indian Ocean. *J. Geophys. Res. Oceans* **123**, 4449–4463 (2018).
43. Rao, R. R. & Sivakumar, R. Seasonal variability of sea surface salinity and salt budget of the mixed layer of the north Indian Ocean. *J. Geophys. Res. Oceans* **108**, 9-1–9-14 (2003).
44. Li, Y. et al. Bay of Bengal salinity stratification and Indian summer monsoon intraseasonal oscillation: 2. Impact on SST and convection. *J. Geophys. Res. Oceans* **122**, 4312–4328 (2017).
45. Carton, J. A., Grodsky, S. A. & Liu, H. Variability of the oceanic mixed layer, 1960–2004. *J. Clim.* **21**, 1029–1047 (2008).
46. Stommel, H. Determination of water mass properties of water pumped down from the Ekman layer to the geostrophic flow below. *Proc. Natl Acad. Sci. USA* **76**, 3051–3055 (1979).
47. Liu, L. L. & Huang, R. X. The global subduction/obduction rates: their interannual and decadal variability. *J. Clim.* **25**, 1096–1115 (2012).
48. Luyten, J. R., Pedlosky, J. & Stommel, H. The ventilated thermocline. *J. Phys. Oceanogr.* **13**, 292–309 (1983).
49. Emery, W. J., Lee, W. G. & Magaard, L. Geographic and seasonal distributions of Brunt–Väisälä frequency and Rossby radii in the North Pacific and North Atlantic. *J. Phys. Oceanogr.* **14**, 294–317 (1984).
50. Timmermans, M.-L. & Marshall, J. Understanding Arctic Ocean circulation: a review of ocean dynamics in a changing climate. *J. Geophys. Res. Oceans* **125**, e2018JC014378 (2020).
51. Lucas, N. S. et al. Giant iceberg meltwater increases upper-ocean stratification and vertical mixing. *Nat. Geosci.* **18**, 305–312 (2025).
52. Srokosz, M. A. & Bryden, H. L. Observing the Atlantic meridional overturning circulation yields a decade of inevitable surprises. *Science* **348**, 1255575 (2015).
53. Broecker, W. S. Unpleasant surprises in the greenhouse? *Nature* **328**, 123–126 (1987).
54. Cheng, L. et al. Improved estimates of ocean heat content from 1960 to 2015. *Sci. Adv.* **3**, e1601545 (2017).
55. Cheng, L. et al. IAPv4 ocean temperature and ocean heat content gridded dataset. *Earth Syst. Sci. Data* **16**, 3517–3546 (2024).
56. Ishii, M. et al. Accuracy of global upper ocean heat content estimation expected from present observational data sets. *Sola* **13**, 163–167 (2017).
57. Levitus, S. et al. World ocean heat content and thermosteric sea level change (0–2000 m), 1955–2010. *Geophys. Res. Lett.* **39**, L10603 (2012).
58. Good, S. A., Martin, M. J. & Rayner, N. A. EN4: quality controlled ocean temperature and salinity profiles and monthly objective analyses with uncertainty estimates. *J. Geophys. Res. Oceans* **118**, 6704–6716 (2013).
59. Durack, P. J., Gleckler, P. J., Landerer, F. W. & Taylor, K. E. Quantifying underestimates of long-term upper-ocean warming. *Nat. Clim. Change* **4**, 999–1005 (2014).
60. Cheng, L. & Zhu, J. Uncertainties of the ocean heat content estimation induced by insufficient vertical resolution of historical ocean subsurface observations. *J. Atmos. Ocean. Technol.* **31**, 1383–1396 (2014).
61. Chen, C. & Wang, G. Role of North Pacific mixed layer in the response of SST annual cycle to global warming. *J. Clim.* **28**, 9451–9458 (2015).
62. Shi, J.-R., Santer, B. D., Kwon, Y.-O. & Wijffels, S. E. The emerging human influence on the seasonal cycle of sea surface temperature. *Nat. Clim. Change* **14**, 364–372 (2024).
63. Liu, F., Song, F. & Luo, Y. Human-induced intensified seasonal cycle of sea surface temperature. *Nat. Commun.* **15**, 3948 (2024).
64. Geng, Y.-F., Xie, S.-P., Zheng, X.-T. & Wang, C.-Y. Seasonal dependency of tropical precipitation change under global warming. *J. Clim.* **33**, 7897–7908 (2020).
65. Song, F., Leung, L. R., Lu, J., Zhou, T. & Huang, P. Advances in understanding the changes of tropical rainfall annual cycle: a review. *Environ. Res. Climate* **2**, 042001 (2023).
66. Zhao, S. et al. Explainable El Niño predictability from climate mode interactions. *Nature* **630**, 891–898 (2024).
67. Li, K.-x & Zheng, F. Effects of a freshening trend on upper-ocean stratification over the central tropical Pacific and their representation by CMIP6 models. *Deep-Sea Res. II* **195**, 104999 (2022).
68. Vincent, E. M., Emanuel, K. A., Lengaigne, M., Vialard, J. & Madec, G. Influence of upper ocean stratification interannual variability on tropical cyclones. *J. Adv. Model. Earth Syst.* **6**, 680–699 (2014).
69. Kumari, A., Kumar, S. P. & Chakraborty, A. Seasonal and interannual variability in the barrier layer of the Bay of Bengal. *J. Geophys. Res. Oceans* **123**, 1001–1015 (2018).
70. Yadidya, B. & Rao, A. D. Interannual variability of internal tides in the Andaman Sea: an effect of Indian Ocean dipole. *Sci. Rep.* **12**, 11104 (2022).
71. Capotondi, A. et al. Mechanisms of tropical Pacific decadal variability. *Nat. Rev. Earth Environ.* **4**, 754–769 (2023).
72. Yang, H. et al. Intensification and poleward shift of subtropical Western Boundary Currents in a warming climate. *J. Geophys. Res. Oceans* **121**, 4928–4945 (2016).
73. Trenary, L. L. & Han, W. Causes of decadal subsurface cooling in the tropical Indian Ocean during 1961–2000. *Geophys. Res. Lett.* **35**, L17602 (2008).
74. Ju, W.-S., Zhang, Y. & Du, Y. Subsurface cooling in the tropical Pacific under a warming climate. *J. Geophys. Res. Oceans* **127**, e2021JC018225 (2022).
75. Luo, Y., Liu, F. & Lu, J. Response of the equatorial Pacific thermocline to climate warming. *Ocean Dyn.* **68**, 1419–1429 (2018).
76. Jiang, F., Seager, R. & Cane, M. A. Historical subsurface cooling in the tropical Pacific and its dynamics. *J. Clim.* **37**, 5925–5938 (2024).
77. Li, Y. et al. Long-term trend of the tropical Pacific trade winds under global warming and its causes. *J. Geophys. Res. Oceans* **124**, 2626–2640 (2019).
78. Latif, M. et al. Strengthening atmospheric circulation and trade winds slowed tropical Pacific surface warming. *Commun. Earth Environ.* **4**, 249 (2023).
79. Lu, Y. et al. North Atlantic–Pacific salinity contrast enhanced by wind and ocean warming. *Nat. Clim. Change* **14**, 723–731 (2024).
80. Zhu, C. & Liu, Z. Weakening Atlantic overturning circulation causes South Atlantic salinity pile-up. *Nat. Clim. Change* **10**, 998–1003 (2020).
81. Haumann, F. A., Gruber, N. & Münnich, M. Sea-ice induced Southern Ocean subsurface warming and surface cooling in a warming climate. *AGU Adv.* **1**, e2019AV000132 (2020).
82. Li, Q., England, M. H., Hogg, A. M., Rintoul, S. R. & Morrison, A. K. Abyssal ocean overturning slowdown and warming driven by Antarctic meltwater. *Nature* **615**, 841–847 (2023).
83. Moorman, R., Morrison, A. K. & McC. Hogg, A. Thermal responses to Antarctic ice shelf melt in an eddy-rich global ocean–sea ice model. *J. Clim.* **33**, 6599–6620 (2020).
84. Peralta-Ferriz, C. & Woodgate, R. A. Seasonal and interannual variability of pan-Arctic surface mixed layer properties from 1979 to 2012 from hydrographic data, and the dominance of stratification for multiyear mixed layer depth shoaling. *Prog. Oceanogr.* **134**, 19–53 (2015).
85. Stammerjohn, S. E., Martinson, D. G., Smith, R. C., Yuan, X. & Rind, D. Trends in Antarctic annual sea ice retreat and advance and their relation to El Niño–Southern Oscillation and southern annular mode variability. *J. Geophys. Res. Oceans* https://doi.org/10.1029/2007JC004269 (2008).
86. Simpkins, G. R., Ciasto, L. M. & England, M. H. Observed variations in multidecadal Antarctic sea ice trends during 1979–2012. *Geophys. Res. Lett.* **40**, 3643–3648 (2013).
87. Armour, K. C., Marshall, J., Scott, J. R., Donohoe, A. & Newsom, E. R. Southern Ocean warming delayed by circumpolar upwelling and equatorward transport. *Nat. Geosci.* **9**, 549–554 (2016).
88. Johnson, G. C., Mahmud, A. K. M. S., Macdonald, A. M. & Twining, B. S. Antarctic bottom water warming, freshening, and contraction in the eastern Bellingshausen basin. *Geophys. Res. Lett.* **51**, e2024GL109937 (2024).
89. Sobel, A. H. & Camargo, S. J. Projected future seasonal changes in tropical summer climate. *J. Clim.* **24**, 473–487 (2011).
90. Eyring, V. et al. Overview of the Coupled Model Intercomparison Project phase 6 (CMIP6) experimental design and organization. *Geosci. Model. Dev.* **9**, 1937–1958 (2016).

91. Eyring, V. et al. in *Climate Change 2021: The Physical Science Basis* (eds Masson-Delmotte, V. P. et al.) Ch. 3 (IPCC, Cambridge Univ. Press, 2021).
92. Cabré, A., Marinov, I. & Leung, S. Consistent global responses of marine ecosystems to future climate change across the IPCC AR5 Earth system models. *Clim. Dyn.* **45**, 1253–1280 (2015).
93. Held, I. M. et al. Probing the fast and slow components of global warming by returning abruptly to preindustrial forcing. *J. Clim.* **23**, 2418–2427 (2010).
94. Long, S.-M. et al. Effects of ocean slow response under low warming targets. *J. Clim.* **33**, 477–496 (2020).
95. Jo, A. R. et al. Future amplification of sea surface temperature seasonality due to enhanced ocean stratification. *Geophys. Res. Lett.* **49**, e2022GL098607 (2022).
96. Alexander, M. A. et al. Projected sea surface temperatures over the 21st century: changes in the mean, variability and extremes for large marine ecosystem regions of northern oceans. *Elementa Sci. Anthrop.* https://doi.org/10.1525/elementa.191 (2018).
97. Sathyanarayanan, A., Köhl, A. & Stammer, D. Ocean salinity changes in the global ocean under global warming conditions. Part I: Mechanisms in a strong warming scenario. *J. Clim.* **34**, 8219–8236 (2021).
98. Jahn, A., Holland, M. M. & Kay, J. E. Projections of an ice-free Arctic Ocean. *Nat. Rev. Earth Environ.* **5**, 164–176 (2024).
99. Shu, Q. et al. Arctic Ocean amplification in a warming climate in CMIP6 models. *Sci. Adv.* **8**, eabn9755 (2022).
100. Liu, Y. et al. How well do CMIP6 and CMIP5 models simulate the climatological seasonal variations in ocean salinity? *Adv. Atmos. Sci.* **39**, 1650–1672 (2022).
101. Shu, Q. et al. Arctic Ocean simulations in the CMIP6 Ocean Model Intercomparison Project (OMIP). *Geosci. Model Dev.* **16**, 2539–2563 (2023).
102. Khosravi, N. et al. The Arctic ocean in CMIP6 models: biases and projected changes in temperature and salinity. *Earth's Future* **10**, e2021EF002282 (2022).
103. Muilwijk, M. et al. Divergence in climate model projections of future Arctic atlantification. *J. Clim.* **36**, 1727–1748 (2023).
104. Liu, H., Song, Z., Wang, X. & Misra, V. An ocean perspective on CMIP6 climate model evaluations. *Deep Sea Res. I.* **201**, 105120 (2022).
105. Treguier, A. M. et al. The mixed-layer depth in the Ocean Model Intercomparison Project (OMIP): impact of resolving mesoscale eddies. *Geosci. Model Dev.* **16**, 3849–3872 (2023).
106. Liu, M., Soden, B. J., Vecchi, G. A. & Wang, C. The spread of ocean heat uptake efficiency traced to ocean salinity. *Geophys. Res. Lett.* **50**, e2022GL100171 (2023).
107. Sharma, S. et al. Future Indian Ocean warming patterns. *Nat. Commun.* **14**, 1789 (2023).
108. Purich, A. & Doddridge, E. W. Record low Antarctic sea ice coverage indicates a new sea ice state. *Commun. Earth Environ.* **4**, 314 (2023).
109. Golledge, N. R. et al. Global environmental consequences of twenty-first-century ice-sheet melt. *Nature* **566**, 65–72 (2019).
110. Himmich, K. et al. Drivers of Antarctic sea ice advance. *Nat. Commun.* **14**, 6219 (2023).
111. Bronselaer, B. et al. Change in future climate due to Antarctic meltwater. *Nature* **564**, 53–58 (2018).
112. Toole, J. M. et al. Influences of the ocean surface mixed layer and thermohaline stratification on Arctic sea ice in the central Canada basin. *J. Geophys. Res. Oceans* **115**, C10018 (2010).
113. Long, S.-M., Xie, S.-P., Zheng, X.-T. & Liu, Q. Fast and slow responses to global warming: sea surface temperature and precipitation patterns. *J. Clim.* **27**, 285–299 (2014).
114. Sun, S., Thompson, A. F., Xie, S.-P. & Long, S.-M. Indo-Pacific warming induced by a weakening of the Atlantic meridional overturning circulation. *J. Clim.* **35**, 815–832 (2022).
115. Schaeffer, A. & Roughan, M. Subsurface intensification of marine heatwaves off southeastern Australia: the role of stratification and local winds. *Geophys. Res. Lett.* **44**, 5025–5033 (2017).
116. Scannell, H. A., Johnson, G. C., Thompson, L., Lyman, J. M. & Riser, S. C. Subsurface evolution and persistence of marine heatwaves in the Northeast Pacific. *Geophys. Res. Lett.* **47**, e2020GL090548 (2020).
117. Oliver, E. C. J., Wotherspoon, S. J., Chamberlain, M. A. & Holbrook, N. J. Projected Tasman sea extremes in sea surface temperature through the twenty-first century. *J. Clim.* **27**, 1980–1998 (2014).
118. Bond, N. A., Cronin, M. F., Freeland, H. & Mantua, N. Causes and impacts of the 2014 warm anomaly in the NE Pacific. *Geophys. Res. Lett.* **42**, 3414–3420 (2015).
119. Sen Gupta, A. et al. Drivers and impacts of the most extreme marine heatwave events. *Sci. Rep.* **10**, 19359 (2020).
120. Collins, M. et al. in *Special Report on the Ocean and Cryosphere in a Changing Climate* (eds Pörtner, H. O. et al.) Ch. 6 (IPCC, Cambridge Univ. Press, 2019).
121. Frölicher, T. L., Fischer, E. M. & Gruber, N. Marine heatwaves under global warming. *Nature* **560**, 360–364 (2018).
122. Wyatt, A. S. J. et al. Hidden heatwaves and severe coral bleaching linked to mesoscale eddies and thermocline dynamics. *Nat. Commun.* **14**, 25 (2023).
123. Schaeffer, A., Sen Gupta, A. & Roughan, M. Seasonal stratification and complex local dynamics control the sub-surface structure of marine heatwaves in eastern Australian coastal waters. *Commun. Earth Environ.* **4**, 304 (2023).
124. Holbrook, N. J. et al. A global assessment of marine heatwaves and their drivers. *Nat. Commun.* **10**, 2624 (2019).
125. Köhn, E. E., Vogt, M., Münnich, M. & Gruber, N. On the vertical structure and propagation of marine heatwaves in the eastern Pacific. *J. Geophys. Res. Oceans.* **129**, e2023JC020063 (2024).
126. Amaya, D. J. et al. Are long-term changes in mixed layer depth influencing North Pacific marine heatwaves? *Bull. Am. Meteorol. Soc.* **102**, S59–S66 (2021).
127. Shi, J. et al. Role of mixed layer depth in the location and development of the Northeast Pacific warm blobs. *Geophys. Res. Lett.* **49**, e2022GL098849 (2022).
128. Elzahaby, Y., Schaeffer, A., Roughan, M. & Delaux, S. Why the mixed layer depth matters when diagnosing marine heatwave drivers using a heat budget approach. *Front. Clim.* **4**, 1–15 (2022).
129. Peng, Q. et al. Surface warming–induced global acceleration of upper ocean currents. *Sci. Adv.* **8**, eabj8394 (2022).
130. Hu, S. et al. Deep-reaching acceleration of global mean ocean circulation over the past two decades. *Sci. Adv.* **6**, eaax7727 (2020).
131. Wang, G., Xie, S.-P., Huang, R. X. & Chen, C. Robust warming pattern of global subtropical oceans and its mechanism. *J. Clim.* **28**, 8574–8584 (2015).
132. Peng, Q. et al. Indonesian throughflow slowdown under global warming: remote AMOC effect versus regional surface forcing. *J. Clim.* **36**, 1301–1318 (2023).
133. Zhang, X., Wang, Q. & Mu, M. The impact of global warming on Kuroshio extension and its southern recirculation using CMIP5 experiments with a high-resolution climate model MIROC4h. *Theor. Appl. Climatol.* **127**, 815–827 (2017).
134. Ju, W.-S., Long, S.-M., Xie, S.-P., Wang, G. & Du, Y. Changes in the North Pacific subtropical gyre under 1.5 °C low warming scenario. *Clim. Dyn.* **55**, 3117–3131 (2020).
135. Huang, J.-H., Tseng, Y.-H. & Kuo, Y.-C. Projected changes of Kuroshio in a warming climate. *J. Clim.* **37**, 6475–6489 (2024).
136. Li, Z. & Fedorov, A. V. A slower north equatorial countercurrent but faster equatorial undercurrent in a warming climate. *J. Clim.* **37**, 6627–6640 (2024).
137. Yang, H. et al. Onshore intensification of subtropical Western Boundary Currents in a warming climate. *Nat. Clim. Change* **15**, 301–307 (2025).
138. Chen, C., Wang, G., Xie, S.-P. & Liu, W. Why does global warming weaken the Gulf Stream but intensify the Kuroshio? *J. Clim.* **32**, 7437–7451 (2019).
139. Sévellec, F., Fedorov, A. V. & Liu, W. Arctic sea-ice decline weakens the Atlantic meridional overturning circulation. *Nat. Clim. Change* **7**, 604–610 (2017).
140. Ma, X. et al. Evolving AMOC multidecadal variability under different CO_2 forcings. *Clim. Dyn.* **57**, 593–610 (2021).
141. Yang, Y., Wu, L. & Fang, C. Will global warming suppress north Atlantic tripole decadal variability? *J. Clim.* **25**, 2040–2055 (2012).
142. Liu, W., Liu, Z., Cheng, J. & Hu, H. On the stability of the Atlantic meridional overturning circulation during the last deglaciation. *Clim. Dyn.* **44**, 1257–1275 (2015).
143. Weiffenbach, J. E. et al. Highly stratified mid-Pliocene Southern Ocean in PlioMIP2. *Clim. Past* **20**, 1067–1086 (2024).
144. Liu, Y., Moore, J. K., Primeau, F. & Wang, W. L. Reduced CO_2 uptake and growing nutrient sequestration from slowing overturning circulation. *Nat. Clim. Change* **13**, 83–90 (2023).
145. Wang, S. et al. A more quiescent deep ocean under global warming. *Nat. Clim. Change* **14**, 961–967 (2024).
146. Sun, S., Wu, L. & Qiu, B. Response of the inertial recirculation to intensified stratification in a two-layer quasigeostrophic ocean circulation model. *J. Phys. Oceanogr.* **43**, 1254–1269 (2013).
147. DeCarlo, T. M., Karnauskas, K. B., Davis, K. A. & Wong, G. T. F. Climate modulates internal wave activity in the northern South China Sea. *Geophys. Res. Lett.* **42**, 831–838 (2015).
148. Yang, Z. et al. Enhanced generation of internal tides under global warming. *Nat. Commun.* **15**, 7657 (2024).
149. Opel, L., Schindelegger, M. & Ray, R. D. A likely role for stratification in long-term changes of the global ocean tides. *Commun. Earth Environ.* **5**, 261 (2024).
150. Jithin, A. K. & Francis, P. A. Role of internal tide mixing in keeping the deep Andaman Sea warmer than the Bay of Bengal. *Sci. Rep.* **10**, 11982 (2020).
151. Zhao, Z. Satellite evidence for strengthened M2 internal tides in the past 30 years. *Geophys. Res. Lett.* **50**, e2023GL105764 (2023).
152. Bij de Vaate, I., Slobbe, D. C. & Verlaan, M. Secular trends in global tides derived from satellite radar altimetry. *J. Geophys. Res. Oceans* **127**, e2022JC018845 (2022).
153. Müller, M., Cherniawsky, J. Y., Foreman, M. G. G. & von Storch, J.-S. Seasonal variation of the M2 tide. *Ocean. Dyn.* **64**, 159–177 (2014).
154. Talke, S. A. & Jay, D. A. Changing tides: the role of natural and anthropogenic factors. *Annu. Rev. Mar. Sci.* **12**, 121–151 (2020).
155. Gong, Y. et al. Accelerated internal tides in a warming climate. *Sci. Adv.* **11**, eadq4577 (2025).
156. Guo, Z. et al. Variability of the M2 internal tides in the Luzon Strait under climate change. *Clim. Dyn.* **62**, 5019–5028 (2024).
157. Yadidya, B. & Rao, A. D. Projected climate variability of internal waves in the Andaman Sea. *Commun. Earth Environ.* **3**, 252 (2022).
158. DeVries, T. The ocean carbon cycle. *Annu. Rev. Environ. Resour.* **47**, 317–341 (2022).
159. Parc, L., Bellenger, H., Bopp, L., Perrot, X. & Ho, D. T. Global ocean carbon uptake enhanced by rainfall. *Nat. Geosci.* **17**, 851–857 (2024).
160. Ashton, I. G., Shutler, J. D., Land, P. E., Woolf, D. K. & Quartly, G. D. A sensitivity analysis of the impact of rain on regional and global sea–air fluxes of CO_2. *PLoS One* **11**, e0161105 (2016).
161. Ho, D. T., Bliven, L. F., Wanninkhof, R. & Schlosser, P. The effect of rain on air–water gas exchange. *Tellus B* **49**, 149–158 (1997).
162. Bopp, L. et al. Multiple stressors of ocean ecosystems in the 21st century: projections with CMIP5 models. *Biogeosciences* **10**, 6225–6245 (2013).
163. Keeling, R. F., Körtzinger, A. & Gruber, N. Ocean deoxygenation in a warming world. *Annu. Rev. Mar. Sci.* **2**, 199–229 (2010).
164. Behrenfeld, M. J. et al. Biospheric primary production during an ENSO transition. *Science* **291**, 2594–2597 (2001).

165. Behrenfeld, M. J. et al. Climate-driven trends in contemporary ocean productivity. *Nature* **444**, 752–755 (2006).
166. Shepherd, J. G., Brewer, P. G., Oschlies, A. & Watson, A. J. Ocean ventilation and deoxygenation in a warming world: introduction and overview. *Phil. Trans. R. Soc. A* **375**, 20170240 (2017).
167. Stramma, L., Johnson, G. C., Sprintall, J. & Mohrholz, V. Expanding oxygen-minimum zones in the tropical oceans. *Science* **320**, 655–658 (2008).
168. Fu, W., Randerson, J. T. & Moore, J. K. Climate change impacts on net primary production (NPP) and export production (EP) regulated by increasing stratification and phytoplankton community structure in the CMIP5 models. *Biogeosciences* **13**, 5151–5170 (2016).
169. Lam, V. W. Y. et al. Climate change, tropical fisheries and prospects for sustainable development. *Nat. Rev. Earth Environ.* **1**, 440–454 (2020).
170. Sun, S., Thompson, A. F., Yu, J. & Wu, L. Transient overturning changes cause an upper-ocean nutrient decline in a warming climate. *Nat. Commun.* **15**, 7727 (2024).
171. Kwiatkowski, L. et al. Twenty-first century ocean warming, acidification, deoxygenation, and upper-ocean nutrient and primary production decline from CMIP6 model projections. *Biogeosciences*. **17**, 3439–3470 (2020).
172. Cermeño, P. et al. The role of nutricline depth in regulating the ocean carbon cycle. *Proc. Natl Acad. Sci. USA* **105**, 20344–20349 (2008).
173. Lotze, H. K. et al. Global ensemble projections reveal trophic amplification of ocean biomass declines with climate change. *Proc. Natl Acad. Sci. USA* **116**, 12907–12912 (2019).
174. Bryndum-Buchholz, A. et al. Twenty-first-century climate change impacts on marine animal biomass and ecosystem structure across ocean basins. *Glob. Chang. Biol.* **25**, 459–472 (2019).
175. Tittensor, D. P. et al. Next-generation ensemble projections reveal higher climate risks for marine ecosystems. *Nat. Clim. Chang.* **11**, 973–981 (2021).
176. Reeburgh, W. S. Oceanic methane biogeochemistry. *Chem. Rev.* **107**, 486–513 (2007).
177. Hamdan, L. J. & Wickland, K. P. Methane emissions from oceans, coasts, and freshwater habitats: new perspectives and feedbacks on climate. *Limnol. Oceanogr.* **61**, S3–S12 (2016).
178. McGinnis, D. F., Greinert, J., Artemov, Y., Beaubien, S. E. & Wüest, A. Fate of rising methane bubbles in stratified waters: how much methane reaches the atmosphere? *J. Geophys. Res. Oceans* **111**, C09007 (2006).
179. Weber, T., Wiseman, N. A. & Kock, A. Global ocean methane emissions dominated by shallow coastal waters. *Nat. Commun.* **10**, 4584 (2019).
180. Westbrook, G. K. et al. Escape of methane gas from the seabed along the West Spitsbergen continental margin. *Geophys. Res. Lett.* **36**, L15608 (2009).
181. Novi, L., Bracco, A., Ito, T. & Takano, Y. Evolution of oxygen and stratification and their relationship in the North Pacific Ocean in CMIP6 Earth system models. *Biogeosciences*. **21**, 3985–4005 (2024).
182. Schmidtko, S., Stramma, L. & Visbeck, M. Decline in global oceanic oxygen content during the past five decades. *Nature* **542**, 335–339 (2017).
183. Lachkar, Z., Mehari, M., Al Azhar, M., Lévy, M. & Smith, S. Fast local warming is the main driver of recent deoxygenation in the northern Arabian Sea. *Biogeosciences* **18**, 5831–5849 (2021).
184. Hogikyan, A., Resplandy, L., Liu, M. & Vecchi, G. Hydrological cycle amplification reshapes warming-driven oxygen loss in the Atlantic Ocean. *Nat. Clim. Change* **14**, 82–90 (2024).
185. Shay, L. K., Goni, G. J. & Black, P. G. Effects of a warm oceanic feature on Hurricane Opal. *Mon. Weather Rev.* **128**, 1366–1383 (2000).
186. Trenberth, K. E., Cheng, L., Jacobs, P., Zhang, Y. & Fasullo, J. Hurricane Harvey links to ocean heat content and climate change adaptation. *Earth's Future* **6**, 730–744 (2018).
187. Lin, I.-I. et al. The interaction of Supertyphoon Maemi (2003) with a warm ocean eddy. *Mon. Weather Rev.* **133**, 2635–2649 (2005).
188. Emanuel, K. A. An air–sea interaction theory for tropical cyclones. Part I: Steady-state maintenance. *J. Atmos. Sci.* **43**, 585–605 (1986).
189. Zhang, X., Xu, F., Zhang, J. & Lin, Y. Decrease of annually accumulated tropical cyclone-induced sea surface cooling and diapycnal mixing in recent decades. *Geophys. Res. Lett.* **49**, e2022GL099290 (2022).
190. Balaguru, K. et al. Ocean barrier layers' effect on tropical cyclone intensification. *Proc. Natl Acad. Sci. USA* **109**, 14343–14347 (2012).
191. Balaguru, K., Foltz, G. R., Leung, L. R. & Hagos, S. M. Impact of rainfall on tropical cyclone-induced sea surface cooling. *Geophys. Res. Lett.* **49**, e2022GL098187 (2022).
192. Webster, P. J., Holland, G. J., Curry, J. A. & Chang, H.-R. Changes in tropical cyclone number, duration, and intensity in a warming environment. *Science* **309**, 1844–1846 (2005).
193. Elsner, J. B., Kossin, J. P. & Jagger, T. H. The increasing intensity of the strongest tropical cyclones. *Nature* **455**, 92–95 (2008).
194. Wang, G., Wu, L., Mei, W. & Xie, S.-P. Ocean currents show global intensification of weak tropical cyclones. *Nature* **611**, 496–500 (2022).
195. Mei, W., Xie, S.-P., Primeau, F., McWilliams, J. C. & Pasquero, C. Northwestern Pacific typhoon intensity controlled by changes in ocean temperatures. *Sci. Adv.* **1**, e1500014 (2015).
196. Huang, P., Lin, I. I., Chou, C. & Huang, R.-H. Change in ocean subsurface environment to suppress tropical cyclone intensification under global warming. *Nat. Commun.* **6**, 7188 (2015).
197. Wang, S. & Toumi, R. Recent tropical cyclone changes inferred from ocean surface temperature cold wakes. *Sci. Rep.* **11**, 22269 (2021).
198. Da, N. D., Foltz, G. R. & Balaguru, K. Observed global increases in tropical cyclone-induced ocean cooling and primary production. *Geophys. Res. Lett.* **48**, e2021GL092574 (2021).
199. Ma, Z. et al. Strengthening cold wakes lead to decreasing trend of tropical cyclone rainfall rates relative to background environmental rainfall rates. *Npj Clim. Atmos. Sci.* **6**, 131 (2023).
200. Guan, S. et al. Ocean internal tides suppress tropical cyclones in the South China Sea. *Nat. Commun.* **15**, 3903 (2024).
201. Zhang, L. & Delworth, T. L. Simulated response of the Pacific decadal oscillation to climate change. *J. Clim.* **29**, 5999–6018 (2016).
202. Chelton, D. B., deSzoeke, R. A., Schlax, M. G., El Naggar, K. & Siwertz, N. Geographical variability of the first baroclinic rossby radius of deformation. *J. Phys. Oceanogr.* **28**, 433–460 (1998).
203. Schneider, N., Miller, A. J. & Pierce, D. W. Anatomy of north Pacific decadal variability. *J. Clim.* **15**, 586–605 (2002).
204. Kwon, Y.-O. & Deser, C. North Pacific decadal variability in the community climate system model version 2. *J. Clim.* **20**, 2416–2433 (2007).
205. Li, S. et al. The Pacific Decadal Oscillation less predictable under greenhouse warming. *Nat. Clim. Change* **10**, 30–34 (2020).
206. Zhang, L. et al. The dependence of internal multidecadal variability in the Southern Ocean on the ocean background mean state. *J. Clim.* **34**, 1061–1080 (2021).
207. Mochizuki, T. et al. Pacific Decadal Oscillation hindcasts relevant to near-term climate prediction. *Proc. Natl Acad. Sci.* **107**, 1833–1837 (2010).
208. Timmermann, A. et al. Increased El Niño frequency in a climate model forced by future greenhouse warming. *Nature* **398**, 694–697 (1999).
209. Thual, S., Dewitte, B., An, S.-I., Illig, S. & Ayoub, N. Influence of recent stratification changes on ENSO stability in a conceptual model of the equatorial Pacific. *J. Clim.* **26**, 4790–4802 (2013).
210. An, S.-I. & Jin, F.-F. Collective role of thermocline and zonal advective feedbacks in the ENSO mode. *J. Clim.* **14**, 3421–3432 (2001).
211. Cai, W. et al. Increased variability of eastern Pacific El Niño under greenhouse warming. *Nature* **564**, 201–206 (2018).
212. Cai, W. et al. Increased ENSO sea surface temperature variability under four IPCC emission scenarios. *Nat. Clim. Change* **12**, 228–231 (2022).
213. Cai, W. et al. Increased frequency of extreme La Niña events under greenhouse warming. *Nat. Clim. Change* **5**, 132–137 (2015).
214. Geng, T. et al. Increased occurrences of consecutive La Niña events under global warming. *Nature* **619**, 774–781 (2023).
215. Cai, W. et al. Changing El Niño–Southern Oscillation in a warming climate. *Nat. Rev. Earth Environ.* **2**, 628–644 (2021).
216. Lu, Z. et al. Increased frequency of multi-year El Niño–Southern Oscillation events across the Holocene. *Nat. Geosci.* **18**, 337–343 (2026).
217. Kohyama, T., Hartmann, D. L. & Battisti, D. S. Weakening of nonlinear ENSO under global warming. *Geophys. Res. Lett.* **45**, 8557–8567 (2018).
218. Zheng, X.-T., Hui, C., Han, Z.-W. & Wu, Y. Advanced peak phase of ENSO under global warming. *J. Clim.* **37**, 5271–5289 (2024).
219. Cai, W. et al. Stabilised frequency of extreme positive Indian Ocean Dipole under 1.5 °C warming. *Nat. Commun.* **9**, 1419 (2018).
220. Wang, G. et al. The Indian Ocean Dipole in a warming world. *Nat. Rev. Earth Environ.* **5**, 588–604 (2024).
221. Seager, R., Henderson, N. & Cane, M. Persistent discrepancies between observed and modeled trends in the tropical Pacific Ocean. *J. Clim.* **35**, 4571–4584 (2022).
222. Senapati, B., O'Reilly, C. H. & Robson, J. Pivotal role of mixed-layer depth in tropical Atlantic multidecadal variability. *Geophys. Res. Lett.* **51**, e2024GL110057 (2024).
223. Brovkin, V. et al. Past abrupt changes, tipping points and cascading impacts in the Earth system. *Nat. Geosci.* **14**, 550–558 (2021).
224. Lenton, T. M. et al. Tipping elements in the Earth's climate system. *Proc. Natl Acad. Sci. USA* **105**, 1786–1793 (2008).
225. van Westen, R. M., Kliphuis, M. & Dijkstra, H. A. Physics-based early warning signal shows that AMOC is on tipping course. *Sci. Adv.* **10**, eadk1189 (2024).
226. Ditlevsen, P. & Ditlevsen, S. Warning of a forthcoming collapse of the Atlantic Meridional Overturning Circulation. *Nat. Commun.* **14**, 4254 (2023).
227. Jackson, L. C. et al. The evolution of the north Atlantic Meridional Overturning Circulation since 1980. *Nat. Rev. Earth Environ.* **3**, 241–254 (2022).
228. Armstrong McKay, D. I. et al. Exceeding 1.5 °C global warming could trigger multiple climate tipping points. *Science* **377**, eabn7950 (2022).
229. Liu, W., Xie, S. P., Liu, Z. & Zhu, J. Overlooked possibility of a collapsed Atlantic Meridional Overturning Circulation in warming climate. *Sci. Adv.* **3**, e1601666 (2017).
230. Mann, M. E. Beyond the hockey stick: climate lessons from the common era. *Proc. Natl Acad. Sci. USA* **118**, e2112797118 (2021).
231. Lenderink, G. & Haarsma, R. J. Modeling convective transitions in the presence of sea ice. *J. Phys. Oceanogr.* **26**, 1448–1467 (1996).
232. Drijfhout, S. et al. Catalogue of abrupt shifts in Intergovernmental Panel on Climate Change climate models. *Proc. Natl Acad. Sci. USA* **112**, E5777–E5786 (2015).
233. Abraham, J. P. et al. A review of global ocean temperature observations: implications for ocean heat content estimates and climate change. *Rev. Geophys.* **51**, 450–483 (2013).
234. Meyssignac, B. et al. Measuring global ocean heat content to estimate the Earth energy imbalance. *Front. Mar. Sci.* **6**, 1–31 (2019).
235. Wang, C., Zhang, L., Lee, S.-K., Wu, L. & Mechoso, C. R. A global perspective on CMIP5 climate model biases. *Nat. Clim. Change* **4**, 201–205 (2014).
236. Luo, F., Ying, J., Liu, T. & Chen, D. Origins of Southern Ocean warm sea surface temperature bias in CMIP6 models. *npj Clim. Atmos. Sci.* **6**, 127 (2023).

237. Zelinka, M. D. et al. Causes of higher climate sensitivity in CMIP6 models. *Geophys. Res. Lett.* **47**, e2019GL085782 (2020).
238. Zhou, C., Zelinka, M. D., Dessler, A. E. & Wang, M. Greater committed warming after accounting for the pattern effect. *Nat. Clim. Change* **11**, 132–136 (2021).
239. Armour, K. C. et al. Sea-surface temperature pattern effects have slowed global warming and biased warming-based constraints on climate sensitivity. *Proc. Natl Acad. Sci. USA* **121**, e2312093121 (2024).
240. Sohail, T., Irving, D. B., Zika, J. D., Holmes, R. M. & Church, J. A. Fifty year trends in global ocean heat content traced to surface heat fluxes in the sub-polar ocean. *Geophys. Res. Lett.* **48**, e2020GL091439 (2021).
241. Fox-Kemper, B. et al. Challenges and prospects in ocean circulation models. *Front. Mar. Sci.* **6**, 2019 (2019).
242. Newsom, E., Zanna, L. & Gregory, J. Background pycnocline depth constrains future ocean heat uptake efficiency. *Geophys. Res. Lett.* **50**, e2023GL105673 (2023).
243. Xu, G. et al. Enhanced upper ocean warming projected by the eddy-resolving Community Earth System Model. *Geophys. Res. Lett.* **50**, e2023GL106100 (2023).
244. Terhaar, J., Frölicher, T. L. & Joos, F. Southern Ocean anthropogenic carbon sink constrained by sea surface salinity. *Sci. Adv.* **7**, eabd5964 (2021).
245. Bourgeois, T., Goris, N., Schwinger, J. & Tjiputra, J. F. Stratification constrains future heat and carbon uptake in the Southern Ocean between 30°S and 55°S. *Nat. Commun.* **13**, 340 (2022).
246. Basak, C. et al. Breakup of last glacial deep stratification in the South Pacific. *Science* **359**, 900–904 (2018).
247. Bouttes, N., Roche, D. M. & Paillard, D. Impact of strong deep ocean stratification on the glacial carbon cycle. *Paleoceanography* **24**, PA3203 (2009).
248. Trenberth, K. E. The definition of El Niño. *Bull. Am. Meteorol. Soc.* **78**, 2771–2778 (1997).

Acknowledgements

The authors acknowledge support from the National Natural Science Foundation of China (grant numbers 42206208, 42261134536, 42076208), the International Partnership Program of the Chinese Academy of Sciences (grant no. 060GJHZ2024064MI), Asian Cooperation Fund, the new Cornerstone Science Foundation through the XPLORER PRIZE, Youth Innovation Promotion Association, Chinese Academy of Sciences, National Key Scientific and Technological Infrastructure project 'Earth System Science Numerical Simulator Facility' (EarthLab), Young Talent Support Project of Guangzhou Association for Science and Technology, and Ocean Negative Carbon Emissions (ONCE). They acknowledge the World Climate Research Programme's Working Group on Coupled Modelling, which is responsible for CMIP, and thank the climate modelling groups for producing and making available their model output through the Earth System Grid Federation. Argo data were collected and made freely available by the International Argo Program and the national programmes contributing to it (https://argo.ucsd.edu, https://www.ocean-ops.org). The Argo Program is part of the Global Ocean Observing System. The observation and model data used in this Review are available at http://www.ocean.iap.ac.cn/. NSF-NCAR is sponsored by the US National Science Foundation. The authors acknowledge discussions with F. Liu, Q. Liu, Y. Gong, S. Li and F. Song. The authors also thank W. Cai, G. Wang, C. Wang, Y. Gong, W. Mei and S. Li for providing data in Fig. 7 of this Review, and W. Zhang for processing global-mean surface temperature data from CMIP6 simulations.

Author contributions

All authors contributed to writing and editing the article. L.C. led the overall conceptual design and the activity and led and coordinated the writing in collaboration with K.T. and the editor. L.C., G.L., K.v.S., K.T., M.M. and J.A. jointly designed the structure of this Review. G.L. led the data analyses; Y.L. led the section on regional stratification and its seasonal variation; L.C. led the introduction and summary sections. X.C., H.L., Z.X., M.L., Q.P., G.X., Z.M. and H.Y. led different topics in the consequences section. All authors contributed to reviewing the stratification changes and the impacts, editing the manuscript and analysing the results.

Competing interests

The authors declare no competing interests.

Additional information

Supplementary information The online version contains supplementary material available at https://doi.org/10.1038/s43017-025-00715-5.

Peer review information *Nature Reviews Earth & Environment* thanks Ryohei Yamaguchi, Chellappan Gnanaseelan and the other, anonymous, reviewer(s) for their contribution to the peer review of this work.

Publisher's note Springer Nature remains neutral with regard to jurisdictional claims in published maps and institutional affiliations.

Springer Nature or its licensor (e.g. a society or other partner) holds exclusive rights to this article under a publishing agreement with the author(s) or other rightsholder(s); author self-archiving of the accepted manuscript version of this article is solely governed by the terms of such publishing agreement and applicable law.

© Springer Nature Limited 2025

[1]State Key Laboratory of Earth System Numerical Modeling and Application, Institute of Atmospheric Physics, Chinese Academy of Sciences, Beijing, China. [2]Eco-Environmental Monitoring and Research Center, Pearl River Valley and South China Sea Ecology and Environment Administration, Ministry of Ecology and Environment, Guangzhou, China. [3]Key Laboratory of Marine Hazards Forecasting, Ministry of Natural Resources, Hohai University, Nanjing, China. [4]College of Oceanography, Hohai University, Nanjing, China. [5]Key Laboratory of Ocean Observation and Forecasting & Laboratory of Ocean Circulation and Waves, Institute of Oceanology, Chinese Academy of Sciences, Qingdao, China. [6]Mercator Ocean International, Toulouse, France. [7]National Center for Atmospheric Research, Boulder, CO, USA. [8]Department of Physics, University of Auckland, Auckland, New Zealand. [9]Department of Earth and Environmental Science, University of Pennsylvania, Philadelphia, PA, USA. [10]School of Engineering, University of St. Thomas, St. Paul, MN, USA. [11]Guangdong Key Laboratory of Ocean Remote Sensing, State Key Laboratory of Tropical Oceanography, South China Sea Institute of Oceanology, Chinese Academy of Sciences, Guangzhou, China. [12]Department of Atmospheric Sciences, Yunnan University, Kunming, China. [13]Laboratory for Ocean Dynamics and Climate, Qingdao Marine Science and Technology Center, Qingdao, China. [14]Department of Atmospheric and Oceanic Sciences, Peking University, Beijing, China. [15]Scripps Institution of Oceanography, University of California San Diego, La Jolla, CA, USA. [16]State Key Laboratory of Physical Oceanography, Institute of Oceanographic Instrumentation, Shandong Academy of Sciences, Qingdao, China. [17]Shandong Computer Science Center, Qilu University of Technology (Shandong Academy of Sciences), Jinan, China. [18]College of Meteorology and Oceanography, National University of Defense Technology, Changsha, China. [19]Computer Network Information Center, Chinese Academy of Sciences, Beijing, China.